Title: Astrocyte-to-neuron communication through integrin-engaged Thy-1/CBP/Csk/Src complex triggers neurite retraction via the RhoA/ROCK pathway.

Authors: Maldonado H., Calderon C., Burgos-Bravo F., Kobler O., Zuschratter W., Ramirez O., Härtel S., Schneider P., Quest A.F., Herrera-Molina R. et al.,

Journal: Biochimica et Biophysica Acta. Molecular Cell Research

Year: 2017

Volume: 1864(2)

Pages: 243-254

DOI: 10.1016/j.bbamcr.2016.11.006

Astrocyte-to-neuron communication through integrin-engaged Thy-1/CBP/Csk/Src complex triggers neurite retraction via the RhoA/ROCK pathway

Running title: Thy-1 regulates neuronal cytoskeleton

H. Maldonado[1,2], C. Calderon[1], F. Burgos-Bravo[1,2], O. Kobler[4], W. Zuschratter[4], O. Ramirez[2,3], S. Häertel[2,3], P. Schneider[5], A.F.G. Quest[1], R. Herrera-Molina[4,*], L. Leyton[1,2,*]

[1]Laboratorio de Comunicaciones Celulares, Centro de Estudios Moleculares de la Célula, Advanced Center for Chronic Disease (ACCDiS); Instituto de Ciencias Biomédicas (ICBM), Facultad de Medicina, Universidad de Chile.

[2]Biomedical Neuroscience Institute (BNI); Instituto de Ciencias Biomédicas (ICBM), Facultad de Medicina, Universidad de Chile.

[3]Laboratory of Scientific Image Analysis (SCIAN); Instituto de Ciencias Biomédicas (ICBM), Facultad de Medicina, Universidad de Chile.

[4]Leibniz Institute for Neurobiology, Magdeburg, Germany.

[5]Department of Biochemistry, University of Lausanne, 1066 Epalinges, Switzerland.

***Corresponding authors** (equal contribution):
Rodrigo Herrera-Molina, Ph.D.; rherrera@lin-magdeburg.de
Lisette Leyton, Ph.D.; lleyton@med.uchile.cl
Phone number: +56 2 2978 6832

FUNDING
This work was supported by the Fondos Nacionales de Ciencia y Tecnología [1150744 to LL, 1130250 to AFGQ, 1151029 to SH]; the Comisión Nacional de Investigación Científica y Tecnológica de Chile [24121665 to HM, 21130008 to FBB, FONDAP15130011 to AFGQ, FONDEF D11I1096 and DAAD to SH]; Iniciativas Científicas Milenio [P09-015-F to LL, HM, OR, and SH]; and the Swiss National Science Foundation grant to PS.

ACKNOWLEDGEMENTS
The authors thank Dr. Claudia Tomes for careful reading of the manuscript.

ABSTRACT

Two key proteins for cellular communication between astrocytes and neurons are αvβ3 integrin and the receptor Thy-1. Binding of these molecules in the same (*cis*) or on adjacent (*trans*) cellular membranes induces Thy-1 clustering, triggering actin cytoskeleton remodeling. Molecular events that could explain how the Thy-1-αvβ3 integrin interaction signals have only been studied separately in different cell types, and the detailed transcellular communication and signal transduction pathways involved in neuronal cytoskeleton remodeling remain unresolved. Using biochemical and genetic approaches, single-molecule tracking, and high-resolution nanoscopy, we provide evidence that upon binding to αvβ3 integrin, Thy-1 mobility decreased while Thy-1 nanocluster size increased. This occurred concomitantly with inactivation and exclusion of the non-receptor tyrosine kinase Src from the Thy-1/C-terminal Src kinase (Csk)-binding protein (CBP)/Csk complex. The Src inactivation decreased the p190Rho GTPase activating protein phosphorylation, promoting RhoA activation, cofilin, and myosin light chain II phosphorylation and, consequently, neurite shortening. Finally, silencing the adaptor CBP demonstrated that this protein was a crucial transducer in the Thy-1 signaling cascade. In conclusion, these data support the hypothesis that the Thy-1-CBP-Csk-Src-RhoA-ROCK axis transmitted signals from astrocytic integrin-engaged Thy-1 (*trans*) to the neuronal actin cytoskeleton. Importantly, the β3 integrin in neurons (*cis*) was not found to be crucial to neurite shortening. This is the first study to detail the signaling pathway triggered by αvβ3, the endogenous Thy-1 ligand, highlighting the role of membrane-bound integrins as *trans* acting ligands in astrocyte-neuron communication.

Key words: αvβ3 integrin, RhoA, STED microscopy, GPI-anchored proteins, interaction *in trans,* cell adhesion molecules.

ABBREVIATIONS

Cell adhesion molecules (CAMs); centers of mass (CM); C-terminal Src kinase (Csk)-binding protein (CBP); extracellular matrix (ECM); glycosylphosphatidylinositol (GPI); green fluorescent protein (GFP); myosin light chain II (MLCII); Rho-associated protein kinase (ROCK); Src family kinases (SFKs); stimulated emission depletion (STED).

INTRODUCTION

Information processing in the central nervous system requires active, complex communication among different cell types. Neurons communicate with other neurons and glial cells, such as astrocytes, transmitting signals that result from coordinated events in the cellular network [1-4]. Cell adhesion molecules (CAMs) are important components that mediate cell-to-cell contact among different cell types. Upon engagement, CAMs also play a key role in activating signal transduction pathways, which modify the actin cytoskeleton and affect adhesion, migration, and transcellular communication [5]. A CAM abundantly expressed in the central nervous system is Thy-1, a small glycosylphosphatidylinositol (GPI)-anchored protein that directly interacts with other CAMs, specifically integrins [6]. Due to the GPI tail, Thy-1 is found in cholesterol/sphingolipid-rich microdomains, or "lipid rafts", in the outer leaflet of the plasma membrane [7-9]. Transient protein confinement in these microdomains promotes signaling to the cell interior of receptors that, similarly to Thy-1, do not span the whole plasma membrane. A molecule that reportedly confines Thy-1 transiently in rafts is the C-terminal Src kinase (Csk)-binding protein (CBP) [10], which is an important scaffolding protein that participates in cell signaling [11-13]. Additionally, the CBP intracellular domain becomes highly phosphorylated on tyrosine and interacts with Src family kinases (SFKs) through these sites, including Src and Csk [14,15]. Csk inactivates Src via Y527 phosphorylation, promoting Src exit from lipid rafts and triggering cell signaling [10,16].

Other important intracellular signaling regulators that affect the actin cytoskeleton and regulate transcellular communication are the small Rho GTPases subfamily members and the molecules that regulate them. The p190Rho GTPase activating protein (GAP), a well-known Src substrate [17-19] activated through Src-mediated phosphorylation, controls RhoA activation [20-22]. Once activated, RhoA binds to effectors, such as the Rho-associated protein kinase (ROCK), and regulates myosin light chain II (MLCII) and cofilin phosphorylation, both of which alter actin dynamics [23,24].

We have previously described that interactions between αvβ3 integrin in astrocytes and Thy-1 in neurons induce neurite retraction through signaling mechanisms involving Thy-1 clustering and Src inactivation [25]. However, how Thy-1 and Src communicate across the different plasma membrane layers in neurons and how this signaling translates into neurite shortening is unknown. One possibility is the use of CBP as a Thy-1 transducer in rafts. Additionally, considering that p190RhoGAP is abundantly expressed in the mammalian brain

[17,18] and is activated by Src to inhibit RhoA [20-22], p190RhoGAP and RhoA are considered probable signaling candidates in the αvβ3 integrin-induced, Thy-1-dependent retraction of neuronal processes.

Notably, a receptor-ligand interaction occurs between molecules in two different cells (interaction *in trans*) in this model. In contrast, a recent study performed in fibroblasts showed that a Thy-1-αvβ3 integrin interaction could also occur in the same membrane plane (interaction *in cis*) via CBP and SFKs, controlling actin dynamics and cell adhesion to the extracellular matrix (ECM) [12]. In Fiore's study, Thy-1 interacts with inactive αvβ3 integrin and brings raft components within integrin proximity before binding to ECM ligands. Previous studies considered the role of Thy-1-integrin interaction both *in cis* and *in trans* and speculated regarding the signaling components (which were studied separately in different cell types) that could explain how Thy-1/αvβ3 integrin interaction led to cell responses, but no studies detailed the characterization of transcellular communication and signal transduction involved in cytoskeleton rearrangement in neurons.

Here, we studied the neuronal integrin contribution (*cis* interaction with Thy-1) to the neurite retraction effect cause by astrocyte integrin (*trans* interaction with Thy-1) and the molecular events downstream of Thy-1 in neurons. Combined two-channel, super-resolution stimulated emission depletion (STED) microscopy, single-molecule tracking, and various functional genetic approaches demonstrated that, in response to αvβ3 integrin stimulation *in trans*, Thy-1 clustered in a Thy-1/CBP/Csk complex that regulated Src location and activity. By inhibiting Src activity, the complex also modulates downstream pathways, including the p190RhoGAP/RhoA/ROCK axis, MLCII, and cofilin. Therefore, we characterized a signaling pathway that linked early plasma membrane events to changes in neuronal morphology. Notably, αvβ3 integrin acted as a ligand that elicited neuron signals by binding to a GPI-anchored receptor (*in trans)* independently of the αvβ3 integrin expression in the target cells (*in cis)*.

RESULTS

Our previous studies confirmed that both primary cortical neurons and the neuron-derived cell line CAD undergo neurite retraction when stimulated with either αvβ3 integrin present on the surface of DITNC1 astrocytes or with the αvβ3-Fc fusion protein [25]. Similar models and experimental approaches were employed in this study.

Integrin αvβ3 promotes neurite retraction *in trans*

Reports demonstrate that neuron-astrocyte communication mediated specifically by Thy-1 (in neurons) and αvβ3 integrin (in astrocytes) resulted in neurite retraction [25]. Recently, Thy-1-αvβ3 integrin association was shown occuring in the same cellular plasma membrane plane (*in cis*) in fibroblasts [12]. Considering that αvβ3 integrin is also found in the neuronal plasma membrane [26], the contribution of integrins from astrocytes (*in trans*) and from neurons (*in cis*) on neurite retraction was evaluated. To this end, the β3 integrin chain was silenced in either the astrocyte-derived cell line DITNC1 or the neuron-like CAD cells. First, astrocytes expressing or lacking integrin were plated and incubated until a monolayer was formed. CAD cells were then added to and differentiated over the DITNC1 cell monolayer as indicated (Fig. 1A). Immunoblot analysis displayed that astrocyte β3 integrin levels decreased in cells transfected with a pool of three siRNAs targeting β3 integrin (Fig. 1B). The results indicate that CAD cells differentiated over DITNC1 cells lacking β3 integrin (siβ3) grew larger neurites than CAD cells differentiated over wild type, non-transfected DITNC1 cells (control) or over DITNC1 cells transfected with a control siRNA (siControl) (Fig. 1C). These results, in conjunction with previous reports indicating that CAD cells lacking Thy-1 (by silencing with shRNA or cleavage with PI-PLC-treatment) are resistant to the effect of αvβ3 integrin on neurite length [25], suggested that αvβ3 integrin promoted neurite retraction by acting as a Thy-1 ligand, *in trans*. To explore whether endogenous integrin present in the neuronal surface also influenced the effect of αvβ3 integrin on neurons, neurite retraction caused by αvβ3 addition to differentiated CAD cells expressing (siControl) or lacking (siβ3) the β3 integrin subunit was evaluated (Fig. 1D). The absence of β3 integrin in the siRNA transfected CAD cells was initially corroborated by Western blot analysis (Fig. 1E). Then, soluble αvβ3 integrin was added to CAD cells expressing (siControl) or lacking (siβ3) the integrin. The results displayed that both CAD cell populations retracted neurites upon addition of soluble αvβ3 integrin, independently of the β3 integrin presence (Fig. 1F). Two conclusions could be drawn from

these results: 1) β3 integrin expressed by the neuronal cells did not participate in neurite retraction and 2) αvβ3 integrin promoted neurite shortening when acting *in trans* as a ligand for Thy-1.

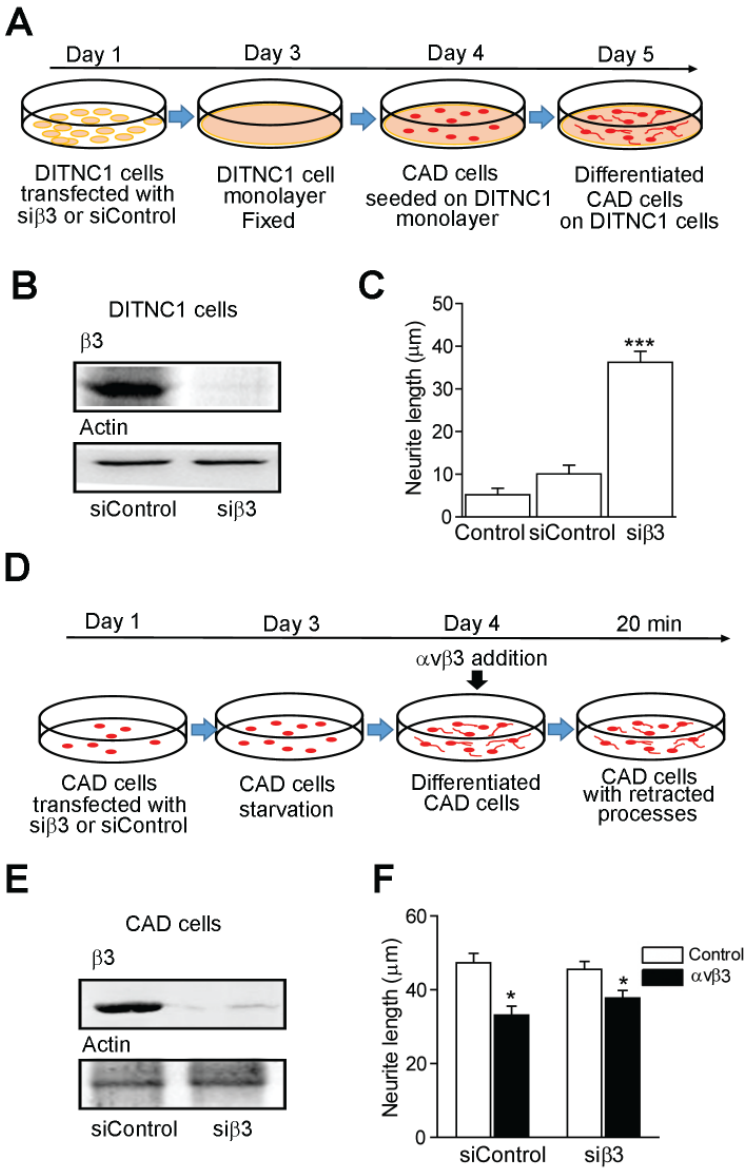

Figure 1: The αvβ3 integrin effect on neurite retraction in a ligand-induced transactivation of Thy-1

(A) DITNC1 cells were transfected with siRNA against the β3 integrin subunit or with siRNA control (day 1), grown as a monolayer, and fixed (day 3). Later (day 4), CAD cells were seeded over the DITNC1 cell monolayer and differentiated during 24 h (day 5). **(B)** Total DITNC1 lysates were immunoblotted for the presence of β3 integrin and actin as a loading control. **(C)** Neurite outgrowth measurements (μm) of differentiated CAD cells over DITNC1 cells (control), β3 integrin-silenced cells (siβ3), or siRNA control cells (siControl). **(D)** CAD cells were transfected to silence β3 integrin expression (day 1). Cells were grown for 2 days (day 3) and differentiated (day 4). Upon differentiation, CAD cells were stimulated or not with αvβ3 integrin. **(E)** Total lysates obtained from transfected or control CAD cells were immunoblotted for β3 integrin expression and actin as a loading control. **(F)** Neurite retraction

analysis (μm) of CAD cells, expressing or lacking β3 integrin, stimulated (black bars) or not (white bars) with αvβ3 integrin. The quantification in C and F is expressed as mean ± SEM of three independent experiments. The neurites of 100 cells were measured per condition, per experiment. *$p < 0.05$, ***$p < 0.001$.

Integrin αvβ3 reduces Thy-1 mobility and velocity, leading to Thy-1 clustering in cortical neurons

Considering that only integrin *in trans* contributed to the neuronal response caused by Thy-1 binding, the downstream signaling events involved in this response necessitated further study, particularly because Thy-1 is a GPI-anchor protein and, as such, does not communicate directly with the cell interior. The effect of Thy-1-αvβ3 integrin binding on Thy-1 movement and velocity was initially assessed because GPI-anchored proteins move more rapidly in the plasma membrane than transmembrane proteins [27,28]. Using cortical neurons stimulated with αvβ3-Fc integrin, individual Thy-1 molecules were followed using high-speed imaging to track anti-Thy-1 antibodies bound to quantum dots (Thy-1-QD). Thy-1-QD movements were followed for 33 s of integrin stimulation and QD images (Fig. 2A, raw) were superimposed to obtain individual molecule-in-time projections {Fig. 2A, projection, color-code: molecules pass fewer (red) or more (yellow) times through the same position} and trajectories (Fig. 2A, tracking). Parameters such as velocity and displacement were determined by tracking individual Thy-1-QD movement. The addition of αvβ3-Fc integrin reduced the Thy-1 molecule velocity (Fig. 2A, B), which was confirmed by the mean velocity quantification of individual molecule tracks (Fig. 2B). Furthermore, the combined projection of all molecule tracks was used to calculate the Thy-1 confinement area, which revealed that the molecule was restrained to areas of ~2 μm^2 in the presence of integrin (Fig. 2C). All data were then collected, and the velocity of individual Thy-1 molecules was assessed and displayed in frequency histogram profiles to reveal differences between the control and treated cells (Fig. 2D). The Thy-1 molecules with reduced mobility (slower than 5 μm/s) increased with the addition of αvβ3 integrin while the faster-moving population (faster than 5 μm/s) decreased ($\chi 2 < 0.0001$) (Fig. 2D).

Considering the Thy-1 movement reduction after αvβ3 integrin binding, this study first demonstrated that Super resolution STED microscopy reproduced and improved previous results regarding Thy-1 cluster formation obtained with a 220 nm XY axial resolution by epifluorescence microscopy [25]. The capacity of the STED microscope to optically resolve individual Thy-1 nanoclusters as small as 40 nm to 50 nm in size was confirmed using two different STED-compatible dyes and image deconvolution procedures

(Supplementary Fig. S1). Then, cluster formation, as well as Thy-1 cluster area and intensity, were evaluated in dendrites. Larger aggregates of higher intensity were observed in αvβ3 integrin-treated cortical neurons than in control neurons (Fig. 2E). The STED image quantification confirmed that stimulation with αvβ3 integrin promoted the formation of larger Thy-1 nanoclusters with higher fluorescence intensity (Fig. 2F).

Together, these results indicate that, with the addition of αvβ3-Fc integrin, Thy-1 molecules forming small clusters reduced mobility, which confined the clusters in microdomains to form larger, higher fluorescence intensity clusters.

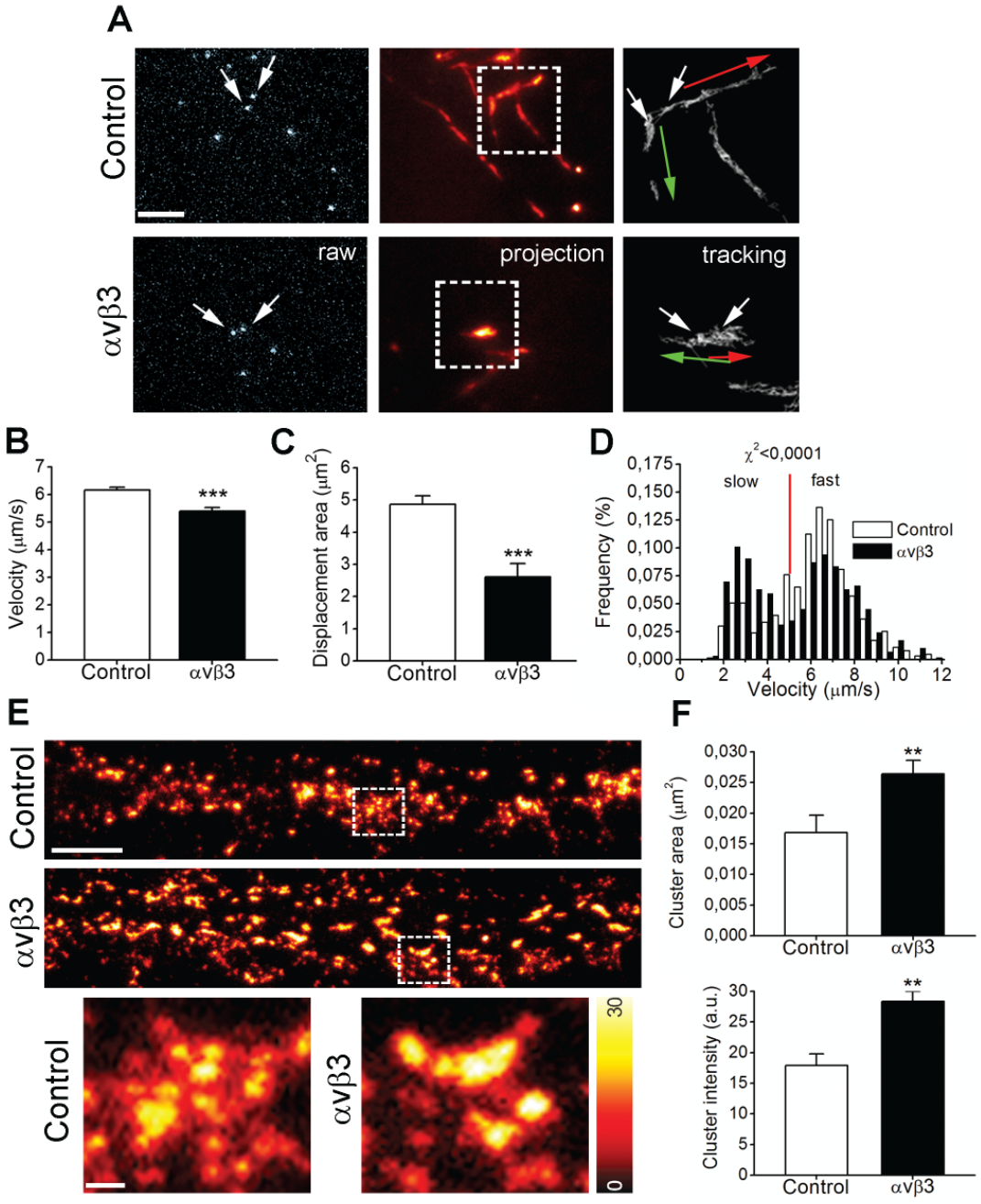

Figure 2: αvβ3 integrin promotes Thy-1 clustering and decreases Thy-1 mobility in the

neuronal plasma membrane

Cortical neurons were treated with αvβ3 integrin-containing (αvβ3) or control (Control) supernatant for 15 min (A–D) or 20 min (E–F). **(A)** Anti-Thy-1 antibody-conjugated quantum dot (Thy-1-QD) movements were followed during the last 33 s of integrin stimulation. The QD images in raw data format (raw), time projections (projection), and trajectories (tracking) are shown. White arrows indicate comparable Thy-1-QDs under different conditions. Red and green arrows indicate the tracked trajectory directions of each Thy-1-QDs. Superimposition of raw QD images (projections) defined the time-dependent trajectories of individual molecules, and parameters were determined by measuring the area enclosing these projections (see boxes). Fully immobile QDs were routinely excluded from analysis. Scale bar = 1.5 μm. **(B–D)** Velocity quantification (B), displacement area (C), and velocity distribution of Thy-1-QD molecules (D) bound to the plasma membrane of control (white bars) and stimulated neurons (black bars). The velocity distribution in (D) identifies a slow- and fast-moving particle subpopulation, as indicated by the red line (cut-off point of 5 μm/s; $\chi^2 < 0.0001$). Values in (B) and (C) are expressed as mean ± standard error of the mean (SEM) from three independent experiments. **(E)** STED images of Thy-1 nanoclusters in dendrites from stimulated and control neurons. Scale bar = 2 μm. A digital zoom of the dashed line squares is shown in the bottom panels. Scale bar = 150 nm. Heat-map scale of cluster fluorescence intensity is presented in arbitrary units (a.u.). **(F)** Area quantification and fluorescence intensity of Thy-1 nanoclusters from STED images. Values are mean ± SEM of five independent experiments (14 images analyzed per condition, per experiment). $^{**}p < 0.01$, $^{***}p < 0.001$ for αvβ3 versus control.

Thy-1, CBP, Csk, and Src form membrane complexes in neurons

Other molecules in Thy-1 microdomains, such as CBP, are also known to mediate Thy-1 confinement and transduce Thy-1 signaling [10]. However, the role of CBP as a Thy-1-transducer molecule that uses integrin as a ligand, or any other natural agonist, has not been studied. Therefore, we tested whether Thy-1 associated with CBP upon addition of αvβ3 integrin, and used STED microscopy and image deconvolution to study Thy-1 and CBP co-localization in neuronal membranes. The co-localization of both molecules increased significantly after 20 min of stimulation with αvβ3 integrin (Fig. 3A, B), showing a clear overlap between Thy-1 and CBP in fluorescence intensity (Fig. 3A). To confirm these results, the distance between the co-localized Thy-1 and CBP cluster centers of mass (CM) was estimated. The Thy-1-CBP clusters were detected at a higher frequency post-integrin treatment (Fig. 3C), indicating reduced mean CM-CM distances between Thy-1 and CBP clusters (Fig. 3C, insert). To gain further insight into the recruitment of Thy-1 and CBP to the same nanodomain, additional criteria were applied to analyze deconvolved STED images (Table 1). These studies assessed cluster intensity, distance to the closest neighboring cluster formed by the same protein (e.g., Thy-1 to the closest Thy-1), cluster area, and cluster density for each independent Thy-1 or CBP channel (Table 1). Consistently, Thy-1 clusters were larger and brighter in integrin-stimulated neurons (Table

1, Fig. 2). The CBP cluster fluorescence intensity, but not the area, also increased (Table 1). Again, CM distances were reduced between Thy-1/Thy-1 but were unchanged between CBP/CBP after integrin addition (Table 1). Moreover, Thy-1 cluster density increased, while the CBP cluster density remained unaltered in stimulated neurons (Table 1).

CBP possesses a cytoplasmic domain that upon phosphorylation interacts with SFK proteins, including Src and Csk [14,15]. Csk inactivates Src, promoting Src exit from lipid raft membrane microdomains [10,16]. Therefore, whether Thy-1-mediated regulation of Src activity depended on CBP/Csk binding was explored. Assessment of Csk co-localization with CBP after integrin stimulation demonstrated that CBP-Csk co-localization increased in cortical neurons (Fig. 3D). Moreover, shorter distances between CBP and Csk clusters were more frequent (Fig. 3E), indicating reduced mean CM-CM distances between these two cluster types upon integrin addition (Fig. 3E, insert). Further image analyses revealed that integrin decreased the area and increased Csk fluorescence intensity (Table 1). However, the distance among Csk puncta (Csk-Csk) did not change. After corroborating the potential interaction between CBP and Csk, the co-localization between CBP and Src in αvβ3 integrin-stimulated cortical neurons was evaluated. CBP-Src co-localization decreased significantly after integrin stimulation (Fig. 3F). The distance between the CBP CM and the Src CM (Fig. 3G), as well as the distance between Src molecules, increased after 20 min of stimulation (Table 1). Neither the area nor the intensity of Src puncta fluorescence was affected by integrin (Table 1).

Finally, to confirm the existence of the Thy-1/CBP/Csk/Src complex in neurons, additional immunoprecipitation experiments were performed using cell lysates obtained from integrin-stimulated or non-stimulated cortical neurons. Immunoprecipitation of Thy-1 showed that Thy-1 co-precipitated with CBP and Src under both stimulated and non-stimulated conditions (Figure 3H). After CBP immunoprecipitation, Thy-1 and Src were detected in the complex with Csk (Fig. 3H). No differences in the Thy-1/CBP/Csk/Src complex were observed upon integrin stimulation (Fig. 3H).

Immunoprecipitation experiments revealed the existence of pre-formed protein complexes that typically did not undergo changes when integrin was added. Importantly, however, local changes in the composition of these complexes were detected with super resolution microscopy, a technique that detects molecules at a nanoscale level [29,30]. Together, these results indicate that upon addition of αvβ3 integrin, Thy-1 clusters moved towards tightly packaged, regularly spaced/less mobile CBP molecules. Additionally, more Csk molecules localized to the plasma membrane and bound to compacted CBP protein in

microdomains. A Src population in these complexes was excluded from CBP microdomains.

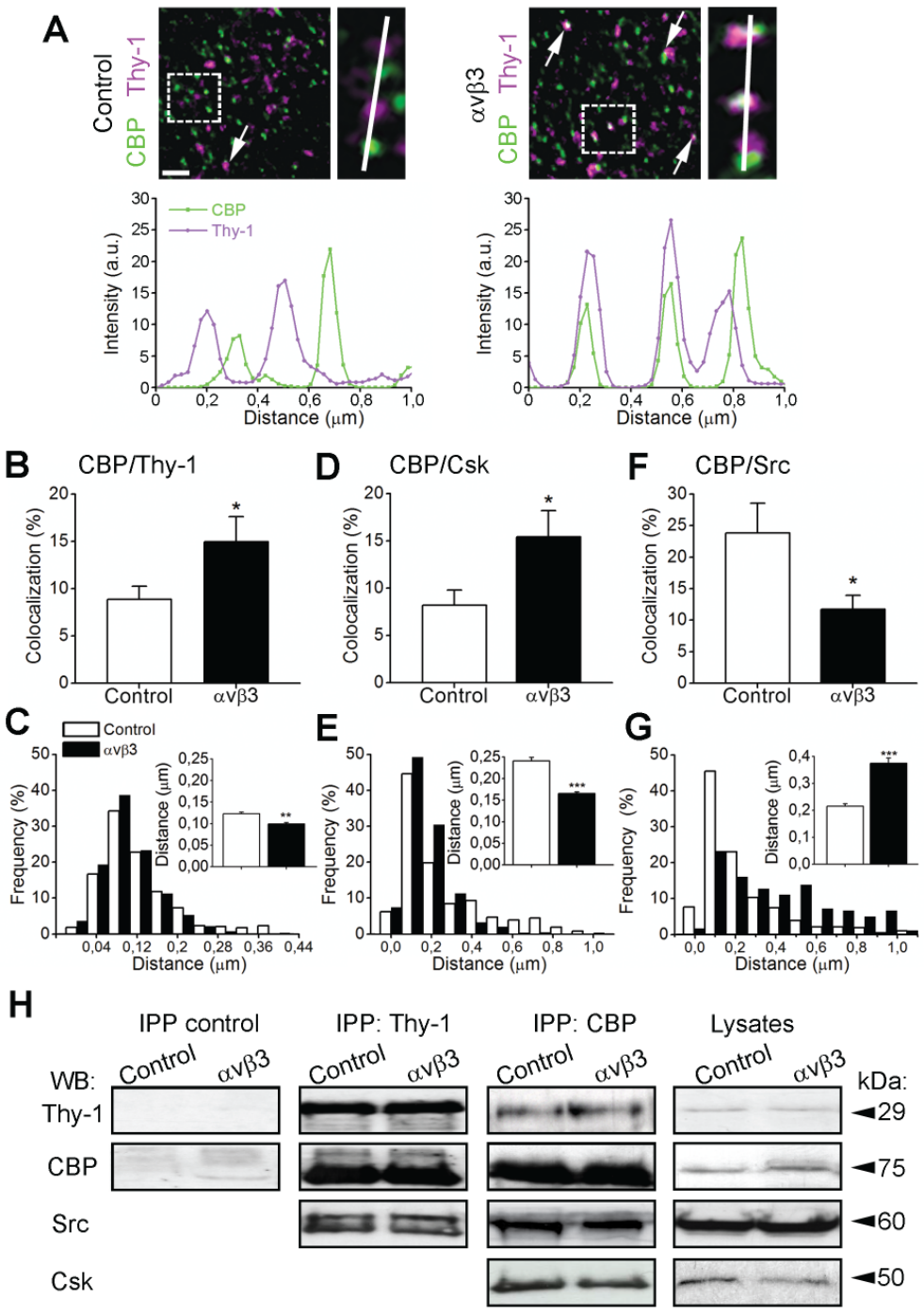

Figure 3: Effects of αvβ3 integrin on Thy-1/CBP, CBP/Src, and CBP/Csk distribution and co-localization in neurons

(A) Immunofluorescence of Thy-1 (magenta) and CBP (green) clusters were obtained by STED microscopy followed by image deconvolution (Huygens software) of control or integrin-stimulated neurons (αvβ3) for 20 min. White arrows indicate co-localized Thy-1-CBP clusters. Digital zoom of dashed-line areas are shown. Scale bar = 0.5 µm. Graphs shown are the Thy-1 and CBP fluorescence intensity profiles over a 1 µm-distance along line scans (white lines on the right side images; scanning starts from the top). **(B, D, and F)** Percentages of CBP co-localization with Thy-1 (B), Csk (D), or Src (F) were calculated

from deconvolved STED images using Imaris software. **(C, E, and G)** Distance between the CM of co-localized clusters of CBP and Thy-1 (C), Csk (E), or Src (G) calculated from deconvolved STED images. Values show the co-localized cluster relative frequency at a given distance. Insert graphs compare the mean distance between the CM of co-localized proteins for each condition. Values are mean ± SEM of 30 STED images taken from three independent experiments; *p < 0.05, **p < 0.01, ***p < 0.001 for αvβ3 versus control. **(H)** Western blots (WB) for Thy-1, CBP, Src, and Csk. Whole-cell lysates were obtained from control or αvβ3 integrin-stimulated neurons and immunoprecipitated with anti-Thy-1 or anti-CBP antibodies. Immunoblots of total lysates and control precipitates that were obtained using a non-related antibody (IPP control) are also shown. Molecular weights (kDa) are indicated.

Thy-1 clustering induced by αvβ3 integrin coincides with Src inactivation

The STED analysis revealed that Src was part of the Thy-1/CBP/Csk complex but that the addition of integrin led to partial exclusion from the complex (Fig. 3). Numerous reports have also linked Thy-1-induced changes to Src activity modulation in different cell types [31-35]. Additionally, Csk inactivates Src via phosphorylation on Y527 [10,16]. To investigate whether the dynamic association of the Thy-1/CBP/Csk complex with Src regulates Src activity, the kinetics of Src phosphorylation on Y527 (Src pY527) in αvβ3 integrin-stimulated cortical neurons were analyzed. The stimulation transiently increased Src pY527 with a peak at 20 min and a return to basal levels at 40 min (Fig. 4A). This kinetics coincided with the maximal increase in the number, size, and intensity of Thy-1 nanoclusters [25] (Fig. 2, Table 1). Changes in cortical neuron Src pY527 were also evaluated by STED microscopy after 20 min of stimulation. Analysis of fluorescence intensity profiles across Src pY527 and Thy-1 signals revealed that plasma membrane-associated Src pY527 appeared in discrete puncta (Fig. 4B). Both intensity and area significantly increased upon treatment with αvβ3 integrin (Table 1). Thy-1-Src pY527 co-localization also increased from 5% to 12% (Fig. 4C), and Thy-1-to-Src pY527 (Fig. 4D) and Src pY527-to-Src pY527 CM distances increased after integrin treatment (Table 1). Notably, upon integrin addition, the Thy-1-Src pY527 CM-CM distance (0.133 ± 0.003 μm, Fig. 4D) was greater than that calculated for Thy-1-CBP (0.099 ± 0.002 μm, Fig. 3C). These data suggest that upon integrin stimulation, an inactive Src population co-localized with Thy-1 molecules in separate clusters that were excluded from the core Thy-1/CBP/Csk complex.

	Area (µm^2)		Intensity (a.u)		CM-CM distance (µm)		Density (n°/µm^2)	
	control	αvβ3	control	αvβ3	control	αvβ3	control	αvβ3
Thy-1	0.009 ± 0.001	0.015 ± 0.002**	12.9 ± 1.2	17.9 ± 1.1**	0.415 ± 0.004	0.395 ± 0.002***	3.4 ± 0.4	5.3 ± 0.6*
CBP	0.006 ± 0.001	0.007 ± 0.001	7.3 ± 0.4	9.1 ± 0.6*	0.355 ± 0.002	0.353 ± 0.002	6.2 ± 0.5	7.3 ± 0.6
Csk	0.010 ± 0.001	0.006 ± 0.001*	9.6 ± 1.2	13.7 ± 1.4*	0.411 ± 0.004	0.412 ± 0.004	8,1 ± 1.4	9.5 ± 1.6
Src	0.004 ± 0.001	0.005 ± 0.001	6.2 ± 0.9	5.9 ± 0.6	0.465 ± 0.008	0.483 ± 0.006*	7.7 ± 0.7	7.4 ± 0.6
Src pY527	0.004 ± 0.001	0.010 ± 0.003*	8.1 ± 0.9	16.2 ± 2.4**	0.344 ± 0.002	0.321 ± 0.001***	6.6 ± 0.5	8.9 ± 0.5*

Table 1: Levels of the area, intensity, center of mass (CM) to CM distance between nearest signals, and density of clusters for each molecule are shown. Data were calculated from deconvolved STED images, which were obtained from control and αvβ3 integrin-stimulated neurons. Values are mean ± standard error of the mean of three independent experiments (ten pictures were measured per condition, per experiment). *p<0.05, **p<0.01, ***p<0.001 vs. respective controls.

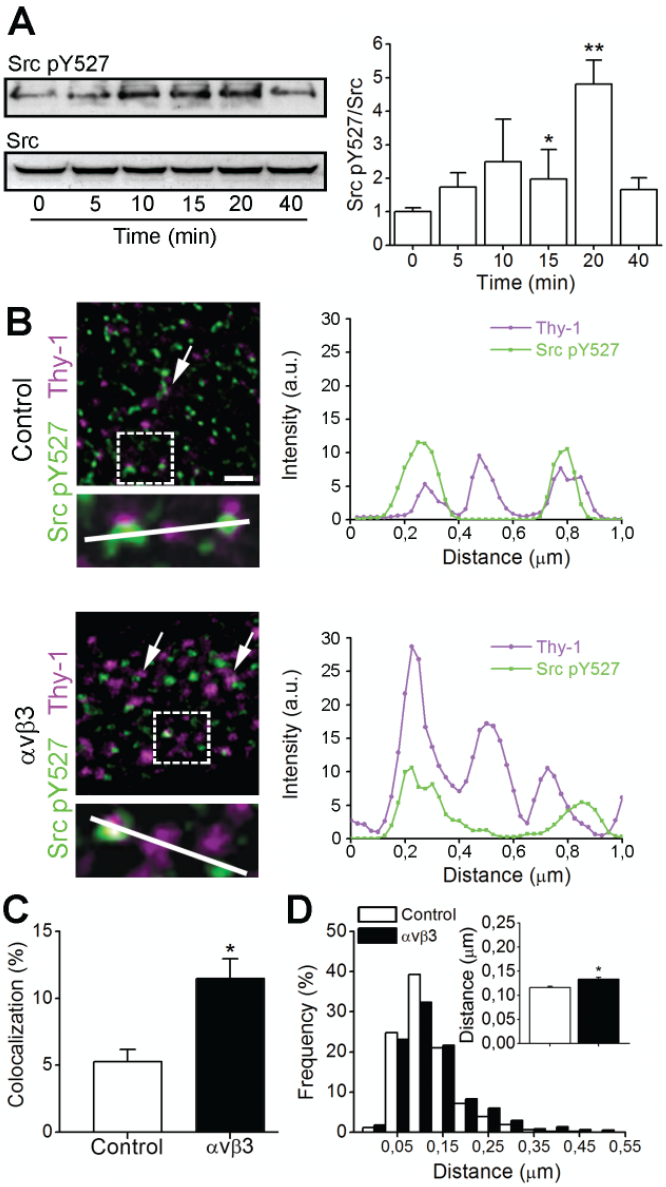

Figure 4: Stimulation with αvβ3 integrin increases Src phosphorylation on Y527 and induces the co-localization of phosphorylated Src with Thy-1 in neurons

(A) Immunoblot of αvβ3 integrin-stimulated neurons at the indicated time periods. The graph shows quantification of the Src pY527/total Src ratio. Values are mean ± SEM of three independent experiments. **(B, C, and D)** Neurons stimulated with (αvβ3) or without (control) αvβ3 integrin for 20 min. **(B)** Deconvolved STED images of Thy-1 (magenta) and Src pY527 (green) nanoclusters. White arrows indicate co-localized clusters. Digital zoom of dashed-line areas are shown (bottom panel). Scale bar = 0.5 μm. White lines (1 μm long) in bottom panels represent line scans where the fluorescence intensity profile of Thy-1 and Src pY527 was quantified (scanning starts from the left). Each scan shows plots of fluorescence intensity versus distance. **(C)** Thy-1-Src pY527 co-localization was calculated from deconvolved STED images. **(D)** Distance between the CM of co-localized clusters of Thy-1 and Src pY527 was calculated from deconvolved STED images as described in Figure 3. Values are presented as mean ± SEM of three independent experiments. In each experiment, 10 neuronal processes were measured per condition. *$p < 0.05$, **$p < 0.01$ for αvβ3 versus control.

The Thy-1/CBP/Csk complex mediates αvβ3 integrin-induced neurite retraction in CAD cells

To prove the functional role of the Thy-1/CBP/Csk complex using cause-effect approaches, the investigation turned from cortical neurons to neuronal-like CAD cells because the CAD cells are simpler to manipulate genetically. First, CAD cell use of similar signaling pathways as cortical neurons when stimulated with integrin ligand was verified. The Thy-1/Src complexes were detected in CAD cells by mass spectrometry assays (Supplementary Fig. S2A). Integrin stimulation enhanced Thy-1-CBP co-localization and diminished CBP-Src co-localization. Both events reached maximum values after 20 min in CAD cells (Supplementary Fig. S2B, S2C, and S2D). The inactivation of Src and neurite shortening was also assessed. Stimulation with αvβ3 integrin increased Src phosphorylation on pY527 (Supplementary Fig. S2E) and decreased neurite length in CAD cells (Supplementary Fig. S2F).

After corroborating that CAD cell response to integrin was similar to the response of cortical neurons, various functional assays (gain and loss of function) with CBP and Src were initiated. First, we determined whether transfection of a constitutively active Src form (Src CA) prevented integrin-induced neurite retraction. Indeed, αvβ3 integrin triggered neurite retraction in mock-transfected CAD cells but not in Src CA-transfected cells, displayed by *in situ* time-lapse microscopy (Fig. 5A). Neurite extension or retraction velocity was quantified from these images. Cells transfected with the control plasmid exhibited a negative velocity (-0.11 μm/min ± 0.02 μm/min) indicative of retraction. In contrast, post-transfection with Src CA, cell processes significantly extended, with a velocity of 0.02 μm/min ± 0.03 μm/min (Fig. 5A). Therefore, integrin-induced neurite retraction required Src inactivation, which was overcome by the expression of a constitutively active Src form.

Considering that the results with cortical neurons indicated that the Thy-1/CBP/Csk core complex regulated Src activity, CBP involvement in neurite retraction and Src inactivation was tested using a small hairpin RNA (shRNA) construct to knock-down CBP (shCBP) in CAD cells. Control cells were transfected with a randomized sequence construct (shScramble). Western blot analysis of cell extracts showed very low CBP levels, but no changes in Thy-1 expression in CBP-knockdown cells (Fig. 5B). Knockdown cells were differentiated and then stimulated with αvβ3 integrin for up to 40 min. CBP silencing prevented integrin-induced neurite retraction (Fig. 5C, gray compared to black bars) and the Src phosphorylation on Y527 (Fig. 5D), confirming the importance of CBP in this pathway.

These results in CAD cells demonstrated the existence of the Thy-1/CBP/Csk complex and revealed the role of CBP as a transducer of Thy-1 signaling in neurons, leading to CBP-dependent Src inactivation. Additionally, CBP and Src were required for αvβ3 integrin-induced neurite retraction.

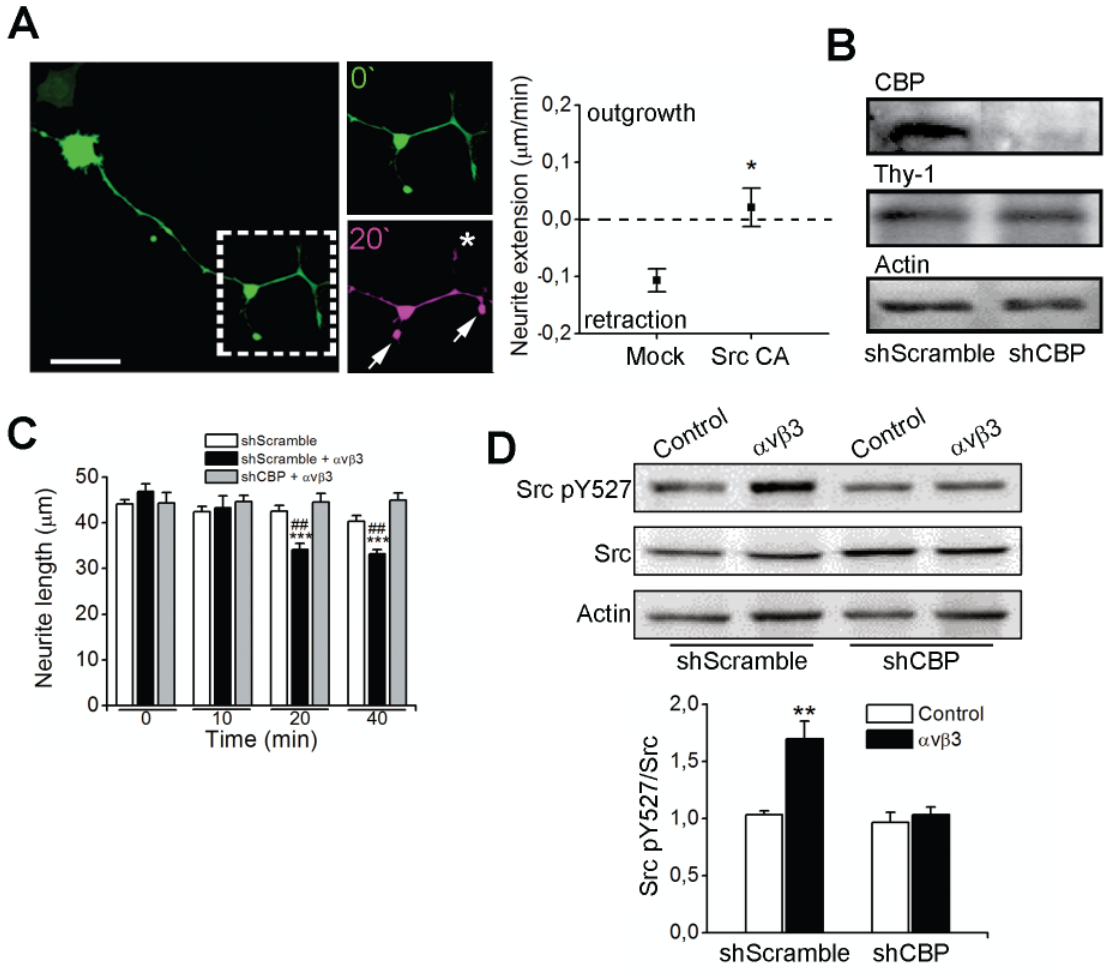

Figure 5: The Thy-1/CBP/Src complex mediates αvβ3 integrin-induced neurite retraction in CAD cells

(A) Differentiated CAD cells were co-transfected with GFP and constitutively active Src (Src CA) or mock control (Mock) plasmids. A whole cell and a digital zoom of control Mock/GFP cell neurite extensions at time points 0 (green) and 20 min of stimulation (magenta) are shown. White arrows and asterisk indicate neurite tip retraction or outgrowth 20 min post-stimulation, respectively. The graph shows the quantification of the total change in neurite length per time unit. Neurite retraction (negative values) and outgrowth (positive values) are displayed for each condition. In each experiment, the neurites of 100 cells were measured per condition. Scale bar = 30 µm. *p < 0.05 versus Mock. **(B)** Immunoblot of cells transfected with CBP small hairpin (sh) RNA (shCBP) or control shRNA (shScramble). **(C)** Quantification of neurite length in shCBP- or shScramble-transfected cells stimulated with αvβ3 integrin. The neurites of 100 cells were measured per condition, per experiment. ***p < 0.001 for shScramble+αvβ3 versus shCBP+αvβ3; ##p < 0.01 for shScramble+αvβ3 versus shScramble. **(D)** Immunoblot of shCBP- or shScramble-transfected cells stimulated with (αvβ3) or without (Control) αvβ3 integrin for 20 min. The graph shows the ratio of Src

pY527/Src, which was normalized to actin. **p < 0.01 for αvβ3 versus control. Values in all graphs are presented as mean ± SEM of three independent experiments

RhoA and ROCK activation function downstream of CBP and are required for αvβ3 integrin-induced neurite retraction

Importantly, p190RhoGAP, a well-known Src substrate [18,36], is abundantly expressed in the mammalian brain, and phosphorylation by Src increases the activity of the substrate [17,18]. The active GAP inactivates RhoA [20-22], a GTPase, which plays a key role in actin cytoskeleton regulation, particularly regarding axonal growth [18]. Therefore, we hypothesized that Src inactivation induced by integrin stimulation of the Thy-1/CBP/Csk complex decreased p190RhoGAP phosphorylation and activated RhoA, triggering neurite shortening. By immunoprecipitating p190RhoGAP, this study found that stimulation with αvβ3 integrin decreased the tyrosine phosphorylation of p190RhoGAP (Fig. 6A). Activation of RhoA was followed by pull-down assays, which showed that active RhoA increased significantly after 20 min of integrin stimulation (Fig. 6B). Fetal bovine serum was used as a positive control for maximal RhoA activation (Fig. 6B). Furthermore, the necessity of RhoA for integrin-induced neurite retraction was tested in CAD cells transfected with plasmids encoding for either GFP alone, GFP fused to a dominant-negative form of RhoA (GFP-DN), or to the Rho-binding domain of a Rho effector (GFP-RBD), which sequesters active RhoA. Though these two RhoA fusion proteins block RhoA activity through different means [37], transfection with either RhoA (GFP-DN) or GFP-RBD, but not with GFP plasmid, prevented integrin-induced neurite shortening, as evaluated by time-lapse microscopy (Fig. 6C, Supplementary Fig. S3A).

The Rho kinase ROCK, an important RhoA effector, modulates the cytoskeleton [38] by regulating the phosphorylation of cytoskeleton-remodeling proteins, including cofilin (Serine 3), a regulator of actin polymerization, and MLCII (Serine 19), a regulator of cytoskeleton contractility [23,24]. Therefore, whether the Thy-1/CBP/Csk/Src complex modulated downstream pathways, including the p190RhoGAP/RhoA/ROCK axis, MLCII, and cofilin substrates, was studied in αvβ3 integrin-stimulated cells. To test this hypothesis, ROCK activity was inhibited by pre-incubating the cells with Y27632. As expected, no neurite shortening was observed in integrin-stimulated cells (Fig. 6D). Additionally, the localization of RhoA and ROCK in the neurites of stimulated and non-stimulated CAD cells was determined through immunofluorescence and confocal microscopy. Following integrin stimulation, RhoA re-distributed to the tip of the processes, while ROCK remained

homogeneously distributed along neurites (Supplementary Fig. S3B). Then, cofilin and MLCII phosphorylation were evaluated by Western blotting. Upon integrin stimulation, cofilin phosphorylation on Serine 3 was increased in CAD cells (Supplementary Fig. S4A) and cortical neurons (Supplementary Fig. S4B). Treatment with integrin also increased MLCII phosphorylation on Serine 19 with similar kinetics in both cell models (Supplementary Figs. S4C, S4D). In summary, stimulation with αvβ3 integrin resulted in p190RhoGAP dephosphorylation, RhoA activation, cofilin and MLCII phosphorylation, and neurite retraction. These results indicate that ROCK is the RhoA effector involved in neurite shortening induced by Thy-1-αvβ3 integrin interaction. Integrin stimulation also induced RhoA redistribution, which may locally activate ROCK to cause neurite retraction.

After confirming integrin stimulation of the RhoA/ROCK/cofilin and RhoA/ROCK/MLCII signaling pathways, CBP modulation of the RhoA/ROCK/cofilin and RhoA/ROCK/MLCII signaling pathways downstream of p190RhoGAP was determined using CAD cells stably transfected with CBP shRNA to connect the core Thy-1/CBP/Csk complex and the aforementioned signal transduction pathways. The results show that CBP silencing prevented the integrin-mediated decrease in p190RhoGAP tyrosine phosphorylation (Fig. 6E), as well as the increase in phosphorylation of both cofilin (Fig. 6F) and MLCII (Fig. 6G). These results confirmed that CBP was an essential component in the events leading to integrin-induced neurite retraction through the p190RhoGAP/RhoA/ROCK axis, and the ROCK downstream effectors cofilin and MLCII, which control the actin cytoskeleton.

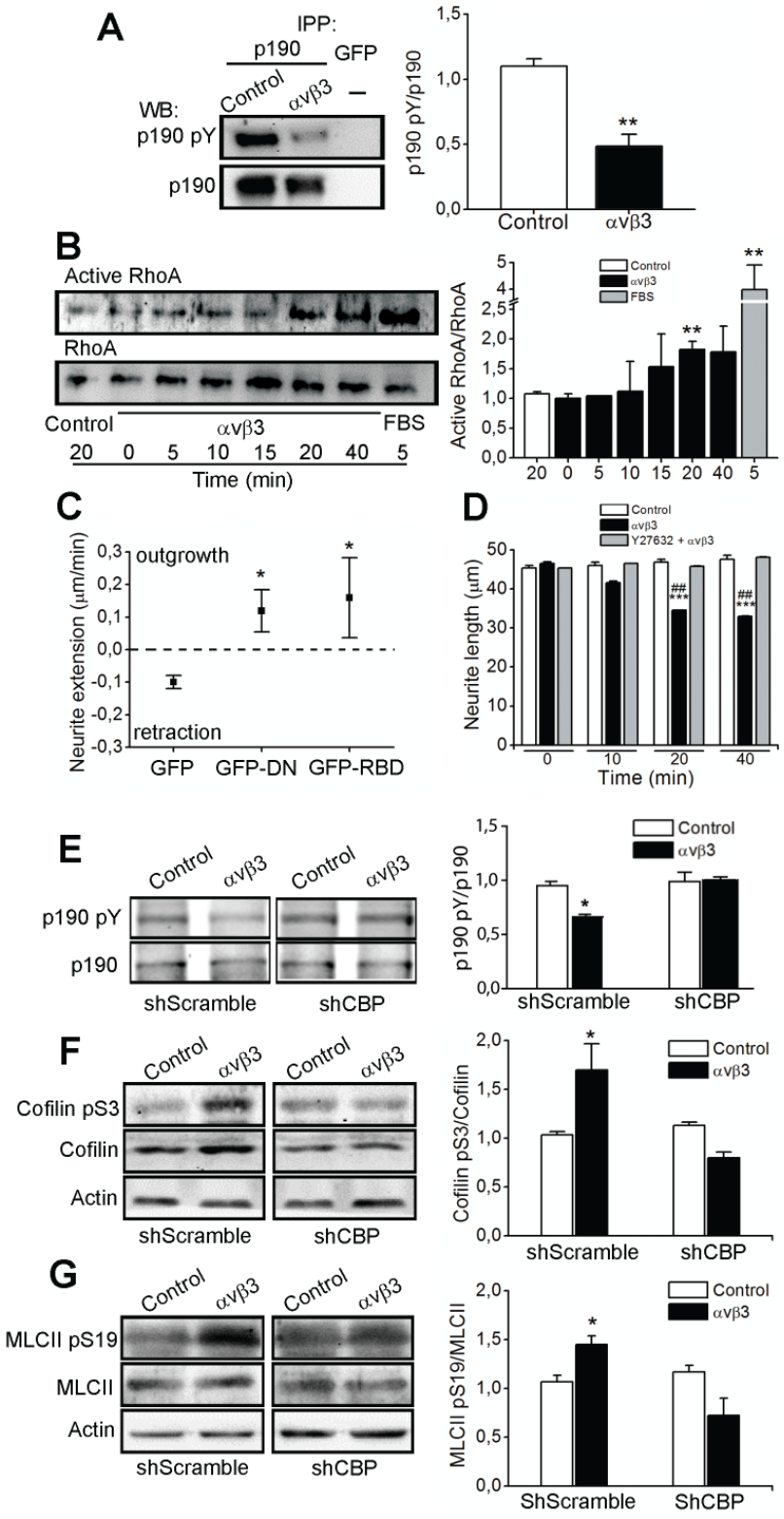

Figure 6: αvβ3 integrin-induced neurite retraction depends on RhoA/ROCK activation downstream of CBP

(A) Lysates from neurons treated with (αvβ3) or without (Control) αvβ3 integrin for 20 min were immunoprecipitated with anti-p190RhoGAP antibody (or anti-GFP antibody as a negative control). Precipitates were run on a gel and immunoblotted for phosphotyrosine (p190 pY) and total p190RhoGAP (p190). The graph shows the quantification of the p190

pY/p190 ratio. **p < 0.01 for αvβ3 versus control. **(B)** Western blot analysis of active RhoA. CAD cells stimulated with αvβ3 integrin for different time periods, treated with control supernatant (Control) or stimulated with 3% FBS (positive control). Values in the graph are the mean of the active RhoA/total RhoA ratio expressed as fold change relative to time 0. **p < 0.01. **(C)** Quantification of neurite length per unit of time from pictures obtained by the time-lapse microscopy of CAD cells transfected with indicated plasmids and stimulated with αvβ3 integrin. The neurites of 100 cells were analyzed per condition, per experiment. *p < 0.05 versus GFP-transfected cells. **(D)** CAD cells pre-incubated with or without the ROCK inhibitor Y27632 and stimulated with αvβ3 integrin-containing (αvβ3) or αvβ3-depleted (Control) supernatant for different time periods. The neurites of 100 cells were measured per condition, per experiment. $^{\#\#}$p < 0.01 for αvβ3 versus control; ***p < 0.001 for αvβ3 versus Y27632+αvβ3. **(E)** Immunoblots and quantification of pY and total p190RhoGAP of whole cell extracts precipitated with anti-p190RhoGAP antibody, performed in shCBP- or shScramble-transfected CAD cells stimulated with αvβ3 integrin. **(F–G)** Immunoblots and quantification of pS3 and total cofilin (E) or pS19 and total MLCII (F) performed in shCBP- or shScramble-transfected CAD cells stimulated with αvβ3 integrin. *p < 0.05 versus control cells. Values in all graphs are mean ± SEM of three independent experiments.

DISCUSSION

The detailed characterization of transcellular communication and signal transduction involved in integrin-induced cytoskeleton rearrangement in neurons remains unresolved. This study described key signaling events downstream of a core membrane complex formed by Thy-1/CBP/Csk in the neuronal membrane. The signals were triggered by αvβ3 integrin ligand binding *in trans* to Thy-1 with no αvβ3 integrin contribution in the neurons. Indeed, αvβ3 integrin from astrocytes or added soluble as αvβ3-Fc integrin, engaged and altered Thy-1 nanocluster dynamic properties, which promoted association with CBP and Csk. This αvβ3 integrin-Thy-1/CBP/Csk complex initiated changes in the localization and activation state of Src kinase, inactivating this tyrosine kinase and consequently decreasing p190RhoGAP activity. A less phosphorylated and inactive p190RhoGAP enhanced the activity of the RhoA/ROCK pathway, the phosphorylation of actin-regulatory proteins, and, as a result, promoted neurite retraction (Fig. 7). These events transduced ligand-coded extracellular information to the cytoskeleton through a signaling cascade downstream of the GPI-anchored protein Thy-1.

Notably, the extracellular information captured by Thy-1 was delivered by an integrin, a molecule typically considered an ECM protein receptor [39,40]. Integrins may act as receptors and ligands, and participate in cell-cell as well as cell-matrix adhesion [41-43]. Moreover, considering that integrins could also interact with proteins present in the same or opposing cells, studies related to cell surface proteins should be interpreted with caution. A recent report describes Thy-1 as a mechanotransduction regulator in fibroblasts because, by interacting with inactive αvβ3 integrin in the membrane plane, Thy-1 controls the ECM effect [12]. In this case, Thy-1-integrin coupling occurs in the same membrane (*cis* interaction) [12]. In other cellular models where Thy-1 and integrin are located in different cells, as is the case for those involved in neuron-astrocyte communication, Thy-1 in neurons activates integrins in astrocytes (*trans* interaction); here, integrins act as Thy-1 receptors that, upon binding, induce focal adhesion and stress fiber formation in astrocytes [42-44]. Alternatively, as shown in the present study, integrin, added soluble or as a cell surface protein, bound to Thy-1 and signaled to the neuronal cytoskeleton inducing neurite shortening (effect *in trans*). Although neurons also expressed αvβ3 integrin on the cell surface, the potential *cis* interaction with Thy-1 appears dispensable for neurite retraction induced *in trans* by the glial αvβ3 integrin. However, the possibility remains that neuronal integrin interacts with both non-clustered Thy-1 *in cis* and inactive Src to regulate Thy-1

signaling (graphical abstract) Therefore, considering that many interactions could occur simultaneously between ECM integrins and proteins, proteins present in the same (*cis)* or in different (*trans)* cells, the complex regulation of CAM functions should be studied using well-designed, controlled experiments (see also [3,9]).

The CAMs that associate to the plasma membrane via a GPI-anchor, including Thy-1, are diffusely distributed on the membrane surface, spontaneously forming small ~2 to 20 molecule nanoclusters [45]. The aggregation of these nanoclusters could be promoted to enhance confinement when GPI-anchored proteins associate with the respective ligands [8,46,47]. Indeed, to induce Thy-1 clustering at least four molecular events could be implicated in facilitating mobility reduction and inducing subsequent confinement**. 1) Endogenous interaction between Thy-1 molecules**. Studies reported direct Thy-1–Thy-1 interactions that depend on a specific sequence located in the periphery of the Thy-1 immunoglobulin-like domain [48-50]. **2) Thy-1-integrin binding.** Thy-1 directly binds integrins, including αMβ2, αXβ2, αvβ5, α5β1, and αvβ3 [43,51-55]. Due to αvβ3 integrin aggregation on the glial cell surface caused by Thy-1 binding [37], restricted Thy-1 lateral diffusion could also result from Thy-1-integrin binding at cell-cell contact sites [6,53] or within the same cell [12]. **3) Association between Thy-1 and CBP in lipid rafts.** CBP is known to reduce Thy-1 lateral mobility in lung fibroblasts [10,56]. **4) Interaction of the Thy-1 membrane complex with the cortical cytoskeleton.** Transmembrane adaptor proteins such as CBP can connect GPI-anchored proteins and the cytoskeleton [46,57].

Our findings describing the existence of a core Thy-1/CBP/Csk complex in the neuronal membrane were consistent with the functional associations between CBP-Thy-1 [10] and CBP-Csk [11,14,15] presented in the literature. Importantly, evidence shows that CBP plays a role in the communication between the surface membrane proteins and the underlying cytoskeleton [10,58,59]. Reports indicate that CBP binds to the Ezrin-Radixin-Moesin-binding protein EBP50 and, through this interaction, associates with Ezrin-Radixin-Moesin, a protein complex directly connected with the actin cytoskeleton [60,61]. No other possible CBP-cytoskeleton links are described for CBP; however, considering that 1) the CBP-EBP50 association is mediated by a PDZ-binding domain that exists in CBP [59,60] and 2) Guanine nucleotide exchange factors, activators of the RhoGTPases, contain PDZ domains, CBP could potentially bind to Guanine nucleotide exchange factors and modulate RhoGTPases activation state. Consequently, CBP downstream of Thy-1 engagement could help transduce signals from surface molecules to the actin cytoskeletal network.

Importantly, mechanically driven changes in Thy-1 mobility, association with CBP,

and other proteins in the complex such as those reported here, as well as the potential link to the actin cytoskeleton are important events for transducing extracellular cues to the cell interior. Our findings demonstrate that integrin-induced Thy-1 clustering in a Thy-1/CBP/Csk complex, which inactivated Src, elicited the p190RhoGAP/RhoA/ROCK axis and triggered neurite retraction. Downregulation of Src severely reduces p190RhoGAP phosphorylation, impairing axon outgrowth, guidance, and fasciculation [18]. Additionally, exacerbated RhoA activation triggers actin destabilization during the contraction or retraction of neuronal processes [21,22,62,63]. The functions of both p190RhoGAP and RhoA are therefore clearly linked to the regulation of neurite extension/retraction. Moreover, our results identified cofilin and MLCII, dynamic regulators of the actin cytoskeleton, as the final mediators of integrin-induced neurite retraction. CBP knockdown completely prevented αvβ3 integrin-induced changes in the phosphorylation status of Src, p190RhoGAP, cofilin, and MLCII. Additionally, αvβ3 integrin did not stimulate the retraction of neuronal processes in cells with reduced CBP levels. Overall, these findings confirmed that CBP was the transmembrane transducer responsible for activating the signaling pathway that regulates actin polymerization, which is initiated by the binding of αvβ3 integrin to Thy-1 *in trans*.

In conclusion, the binding of αvβ3 integrin *in trans* with Thy-1 enhanced molecular clustering and regulated the connectivity between Thy-1 microdomains and CBP/Csk nanoclusters to trigger Src-dependent alterations in the actin cytoskeleton, leading to neurite retraction. For the first time, we uncovered a detailed signaling pathway from Thy-1 engagement to alterations in the actin cytoskeleton of neurons and highlighted the important transcellular communication role of membrane-bound integrins as ligands. Considering that Thy-1 and CBP reside in lipid rafts, our results also shed light on how microdomain dynamics contributed to cell signaling events within the contact interface of astrocyte-neuron associations. This knowledge could open new avenues for the study of CAMs in the brain.

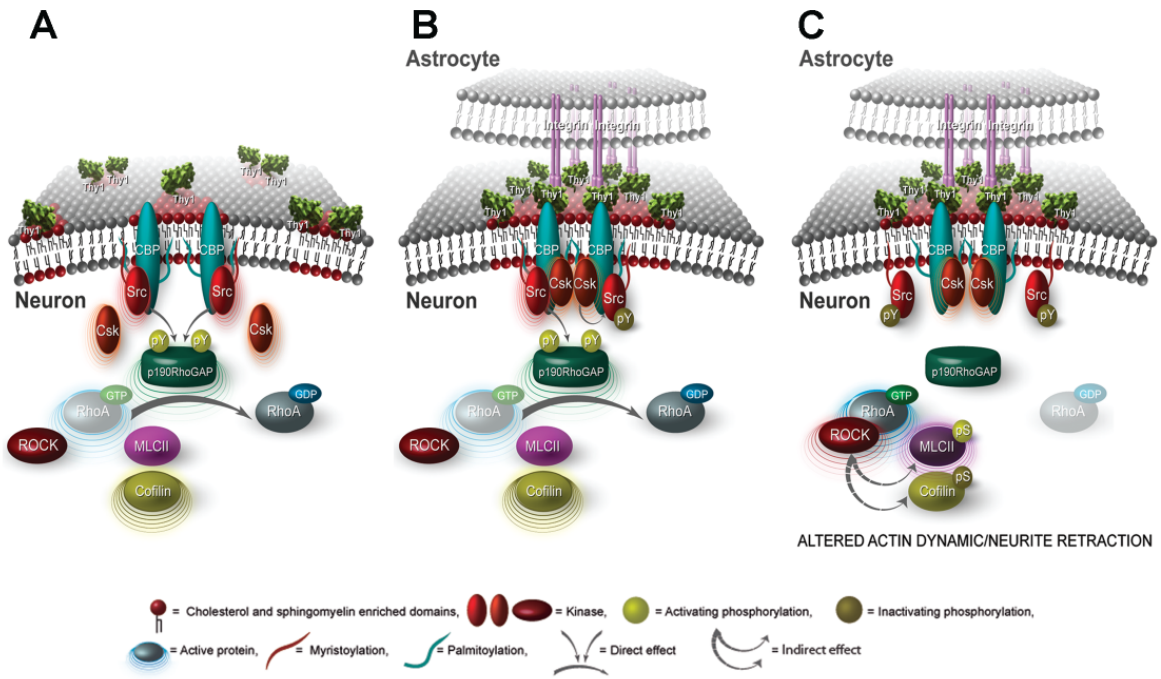

Figure 7: Working model for αvβ3 integrin-induced changes in Thy-1-dependent signaling and cytoskeleton regulation.

(A) Under control conditions, Thy-1 nanoclusters at the plasma membrane were small and dynamically associated or disassociated from CBP in lipid microdomains. When phosphorylated, CBP bound to active Src, and this SFK phosphorylated and activated p190RhoGAP to convert RhoA in the GDP-bound, inactive form. **(B)** Binding of αvβ3 integrin to Thy-1 induced clustering around CBP-Src-containing domains. Csk was then recruited to the Thy-1-CBP-Src complex, where it phosphorylated Src on Y527 and switched off Src activity. **(C)** Inactive Src moved deviated from the Thy-1-CBP-Csk complex, decreasing p190RhoGAP phosphorylation and activation. This increased active GTP-bound RhoA levels that activated ROCK to phosphorylate cofilin and MLCII, altering actin cytoskeleton dynamics and leading to the retraction of neuronal processes.

MATERIALS AND METHODS

Cell cultures and αvβ3-Fc production

CAD cells were maintained and differentiated into a neuronal-like phenotype (at least one neurite per cell, longer than 15 μm) as reported [25]. Purified primary neurons were obtained from brain cortices of 18-day-old rat embryos, according to published protocols [64]. Neurons were seeded on poly-L-lysine-coated plates and then cultured *in vitro* for 14 days as previously reported [25]. All procedures were revised and approved by the local Bioethics Committee for Animal Experimentation at the University of Chile (CBA #0377 and #0790). The DITNC1 astrocytes were maintained in RPMI 1640 (Gibco, Carlsbad, CA, USA) with 5% FBS (Hyclone, Logan, UT, USA) and 0.1 mM 2-mercaptoethanol (Gibco). Recombinant αvβ3-Fc integrin protein was secreted into serum-free cell culture media by co-transfected HEK cells, as previously published [25,51]. CAD and DITNC1 cell lines were periodically checked for mycoplasma contamination using a PCR detection kit (Roche, Basel, Switzerland).

Analysis of neurite length

Differentiated CAD cells were incubated with αvβ3-Fc-containing supernatants diluted in serum-free medium (1:10) for 0 min to 60 min. Control cells were incubated with αvβ3-Fc-depleted supernatants, which were obtained by overnight incubation with 1 mg/ml Protein A-beads (Sigma-Aldrich, St. Louis, MO, USA) at 4 °C. Alternatively, CAD cells were differentiated for 24 h over a confluent monolayer of fixed DITNC1 cells as previously described [25]. In the ROCK experiments, differentiated CAD cells were pretreated with 10 μM Y27632 (Roche) for 1 h and then stimulated with αvβ3 integrin. Neurite length was measured using the NeuronJ plug-in for ImageJ software.

Time-lapse microscopy analyses of neurite length

CAD cells were transfected with the corresponding plasmids using the calcium phosphate technique. To evaluate Src participation, CAD cells were co-transfected with green fluorescent protein (GFP) and either Src CA (which contains a mutation in the inactivating phosphorylation site Y527F) or mock control plasmid. To evaluate RhoA participation, cells were transfected with GFP-RhoA DN (N19-RhoA), GFP-RBD (Rotekin Rho-binding domain), or GFP constructs. For transfections, cells were incubated with 50 μl of 25 mM HEPES (pH 7.05) containing 250 mM $CaCl_2$, 70 mM NaCl, 0.75 mM Na_2PO_4 and 1 μg of DNA in 0.5 ml of DMEM-F12 containing 8% FBS for 4 h. Then, cells were

differentiated for 24 h and incubated with αvβ3-Fc integrin or control (αvβ3-Fc-depleted) supernatants for 1 h at 37 °C. The neurite processes of GFP-positive cells were photographed every 10 min using a FV10i confocal microscope (Olympus Corp., Tokyo, Japan) equipped with a UPLSAPO 60X/1.35 water immersion objective (pixel size: 0.207 μm × 0.207 μm). Neurite length was analyzed using the NeuronJ plug-in.

Immunofluorescence

Cells were fixed with 4% paraformaldehyde in Hank's balanced salt solution (Gibco) for 10 min and then treated with a buffer containing 10% FBS, 0.1 mM glycine, and 0.1% Triton in Hank's balanced salt solution. Primary antibodies were added for 1 h at room temperature: anti-Thy-1 (1:100; BD Biosciences, San Jose, CA, USA), mouse anti-CBP (1:200; Abcam, Cambridge, MA, USA), rabbit anti-CBP (1:400; Abcam), anti-Src (1:200; Cell Signaling Technology, Danvers, MA, USA), anti-Src pY527 (1:200; Cell Signaling), anti-Csk (1:50; EMD Millipore, Billerica, MA, USA), anti-RhoA (1:200; Santa Cruz Biotechnology Inc., Dallas, TX, USA), and anti-ROCK (1:200; Cell Signaling). Samples were washed, and the following secondary antibodies were added for 1 h at room temperature: anti-mouse Alexa 488 (1:400; Life Technologies, Carlsbad, CA, USA), anti-rabbit IgG Alexa 546 (1:200; Life Technologies), anti-mouse IgG or anti-rabbit IgG Abberior Star 580 (1:200; STED; Abberior, Göttingen, Germany), and anti-mouse IgG or anti-rabbit IgG ATTO 647N (1:400; STED; Atto-tec, Siegen, Germany). After washing and mounting the coverslips with 2.5% 1, 4-Diazabicyclo-octane, 10% Mowiol 4-88, 25% glycerol, and 0.1 M Tris-HCl (pH 8.5), the dyes were visualized in an Olympus IX81 Fv1000 confocal microscope with a UPLSAPO 60X/1.35 oil immersion objective and 4× digital zoom (pixel size: 51 nm × 51 nm) or in a Leica TCS STED-SP5 microscope with a HCX PL APO CS 100.0×/1.40 oil immersion objective and 6× digital zoom (voxel size: 25.3 nm × 25.3 nm × 209.8 nm).

Image processing and analyses

STED or confocal images were deconvolved using the "classic maximum likelihood estimator" in the deconvolution toolbox of Huygens professional software (Scientific Volume Imaging B.V., Hilversum, The Netherlands). Images were converted to an 8-bit format, and the threshold was adjusted using Otzu's algorithm in ImageJ. The area and number of clusters were quantified using the ImageJ "analyze particle" tool. Cluster intensity was evaluated directly from STED-deconvolved images using the Imaris software

"spots function tool" (Bitplane, Zurich, Switzerland). The distance between nanocluster CMs from STED-deconvolved images was processed with the "object analyzer advanced tool" (Huygens software). Homo-cluster distances (e.g., Thy-1-Thy-1, CBP-CBP) were analyzed with the "correlation inside channels" option. To analyze hetero-clusters, images were previously filtered using the "remove non-overlapping signals" option, and the distances were estimated with the "correlation between channels" option (Huygens software). Co-localization analyses in both STED and confocal modes were performed using the Imaris co-localization module. Random co-localization was evaluated using the Imaris "automatic threshold" tool.

QD mobility analyses

These experiments were performed according to published protocols [65]. The primary antibody against Thy-1 (1.0 µl, clone OX-7, BD Biosciences) was mixed with 1.0 µl quantum dot (QD) solution (QD655 goat F[ab´]2 anti-rat IgG conjugate, 1 mM; Invitrogen, Carlsbad, CA, USA) in 7.0 µl PBS for 5 min. Subsequently, 1 ml casein (10X Casein Solution; Vector Laboratories Inc., Burlingame, CA, USA) was added for 5 min. An anti-Thy-1-QD 1:1,000 dilution was added to neurons on coverslips that were then incubated for 5 min to 10 min and washed. Time-lapse recordings of QD-labeled Thy-1 were obtained at 35 °C in a perfusion chamber mounted onto an upright microscope (Olympus BX50) equipped with a 60× water immersion objective (NA = 1.1). Images were acquired with a QuantEM 5125C camera (Visitrom System, pixel size: 60 nm × 60 nm). A 430-nm laser was used to excite QDs, and fluorescence emission was collected through a HQ605/40 filter. Time-lapse recordings of QDs were obtained using Metaview software to analyze up to 3,000 consecutive frames with an integration time of 10 ms to 30 ms. The images were first converted to an 8-bit format using ImageJ, and the salt-and-pepper noise reduction was performed using a 2 pixel-radius middle filter. Then, the images were convolved using a 3 pixel-radius Laplacian filter. Objects with a radius < 3 pixels were not considered in the study. Interactive Data Language tracked QD-labeled molecules on randomly selected dendritic regions.

Western blot analyses

Protein extracts were prepared in RIPA buffer {25 mM Tris-HCl (pH 7.6), 150 mM NaCl, 1% NP-40, 1% sodium deoxycholate, 0.1% sodium dodecyl sulfate (SDS)}X, supplemented with PhosSTOP phosphatase (Roche) and protease inhibitor cocktails (Sigma-

Aldrich). Protein extracts were electrophoretically separated in 10% to 15% SDS-PAGE gels and transferred to nitrocellulose (EMD Millipore). The nitrocellulose was blocked with 5% w/v nonfat, dry milk in PBS containing 0.1% Tween-20 and then incubated with the following primary antibodies: anti-Thy-1 (1:1,000) (BD Pharmigen Inc., Franklin Lakes, NJ, USA); anti-CBP (1:1,000) and anti-integrin-β3-chain (1:500) (Abcam); anti-Src (1:2,000), anti-Csk (1:500), and anti-phosphotyrosine (1:1,000) (EMD Millipore); anti-Src phospho Y527 (1:1,000), anti-MLCII (1:1,000), anti-MLCII phospho S19 (1:1,000), anti-Cofilin (1:1,000), and anti-Cofilin phospho S3 (1:1,000) (Cell Signaling); anti-RhoA (1:250) and anti-p190RhoGAP (1:500) (Santa Cruz Biotechnology); and anti-β-actin (1:5,000; Sigma-Aldrich). The membrane was then washed and incubated with horseradish peroxidase-conjugated goat anti-rabbit IgG (1:5000; EMD Millipore) or goat anti-mouse IgG (1:2000; KPL, Gaithersburg, MD, USA) antibody for 1 h at room temperature. Bands were visualized with a Pierce chemiluminescence kit (Thermo Fisher Scientific Inc., Rockford, IL, USA), according to the manufacturer's instructions.

Immunoprecipitation and Maldi-TOF analysis

Differentiated neurons were lysed using a buffer containing 20 mM CHAPS, 50 mM NaCl, 2 mM EGTA, 1 mM PMSF, 1 mM benzamide, and 0.5 mM Na_3VO_4 in 10 mM Tris-OH (pH 7.2). Clarified lysates were incubated with 10 µl of Thy-1 or CBP antibody at 4 °C for 1 h. Then, protein A-coated beads (1 mg/ml) were added for 1 h at 4 °C. After washing, samples were resuspended in SDS Sample Buffer (125 mM Tris-HCl, pH 6.8, 2% glycerol, 4% SDS, and 0.05% bromophenol blue) for Western blot analysis.

Maldi-TOF analysis was performed using the Amino-link Kit (Thermo Fisher Scientific Inc.), according to the manufacturer's instructions. Samples were desiccated in a SpeedVac (Eppendorf, Hamburg, Germany), resuspended in 100 µl of 50 mM NH_4HCO_3, and incubated with 25 µl of 45 mM DTT at 50 °C for 15 min. Iodoacetamide (25 µl, 100 mM) (Sigma-Aldrich) was added for 15 min at room temperature. Finally, porcine trypsin (5 µl) (Roche) was added and incubated overnight at 37 °C. Tryptic peptides were dried using a SpeedVac, centrifuged, and dissolved in 0.1% v/v formic acid. Samples were desalted using ZipTip C18 (EMD Millipore). Mass spectra were acquired in a Microflex MALDI-TOF instrument (Bruker Daltonics, Inc., Billerica, MA, USA) in positive and reflection modes. Data were examined using the Mascot database "peptide mass fingerprint" and "sequence query" tools.

Stably transfected CBP-knockdown cells

CAD cells were stably transfected with a commercial shRNA against CBP (Qiagen, Valencia, CA, USA) or a scrambled plasmid using calcium phosphate (see above). Stably transfected cells were selected using 2 μg/ml puromycin (Sigma-Aldrich) for 2 weeks. After selection, cells were maintained in medium with 0.5 μg/ml puromycin. For experimentation, stably transfected cells were differentiated for 24 h in the absence of puromycin.

Integrin β3-chain silencing

DITNC1 and CAD cells were transfected using siPORT Amine (Thermo Fisher Scientific) according to the manufacturer's protocol with a mix of three different siRNA against αvβ3 integrin β3 chain (5′→3′ GCUACUCAUCACCAUUCAU, GGUGGAGGAUUACCUGUA, GGAGCAAUCUUUCACUAUU) or control siRNA.

RhoA activity assays

For the pull-down assay, differentiated CAD cells were stimulated with or without αvβ3 integrin or 3% FBS (positive control) and then lysed with 500 μl lysis buffer containing 25 mM Tris-HCl (pH 7.2), 150 mM NaCl, 5 mM $MgCl_2$, 1% NP-40, 5% glycerol, and a protease inhibitor cocktail (EMD Millipore) on ice. Then, samples were incubated at 4 °C for 1 h with 50 μl of glutathione-agarose beads coated with GST-RBD. Finally, samples were washed with lysis buffer, centrifuged, and resuspended in SDS sample buffer. Samples were run on gels and immunoblotted with anti-RhoA antibodies.

Statistical analysis

The statistical analysis was performed using GraphPad Prism 5 or SPSS software. Differences between the two groups were assessed using the Student's unpaired t-test (normal distribution) or Mann-Whitney U test (Western blot analysis). Differences between three or more groups were examined using the one-way analysis of variance test with the Tukey-Kramer post hoc analysis. Data normality was corroborated using the Shapiro Wilkinson test. The analysis of QD velocity distribution was assessed using the $\chi 2$ test, with a cut-off point of 5 μm/s. P values < 0.05 were considered statistically significant.

REFERENCES

[1] Kirischuk S, Héja L, Kardos J, Billups B (2015) Astrocyte sodium signaling and the regulation of neurotransmission. Glia: n/a-n/a.

[2] Croft W, Dobson KL, Bellamy TC (2015) Plasticity of Neuron-Glial Transmission: Equipping Glia for Long-Term Integration of Network Activity. Neural Plasticity 2015: 11.

[3] Cardenas A, Kong M, Alvarez A, Maldonado H, Leyton L (2014) Signaling pathways involved in neuron-astrocyte adhesion and migration. Curr Mol Med 14: 275-290.

[4] Fields RD, Burnstock G (2006) Purinergic signalling in neuron-glia interactions. Nat Rev Neurosci 7: 423-436.

[5] Cavallaro U, Dejana E (2011) Adhesion molecule signalling: not always a sticky business. Nat Rev Mol Cell Biol 12: 189-197.

[6] Leyton L, Hagood JS (2014) Thy-1 modulates neurological cell-cell and cell-matrix interactions through multiple molecular interactions. Adv Neurobiol 8: 3-20.

[7] Barker TH, Hagood JS (2009) Getting a grip on Thy-1 signaling. Biochim Biophys Acta 1793: 921-923.

[8] Brugger B, Graham C, Leibrecht I, Mombelli E, Jen A, et al. (2004) The membrane domains occupied by glycosylphosphatidylinositol-anchored prion protein and Thy-1 differ in lipid composition. J Biol Chem 279: 7530-7536.

[9] Herrera-Molina R, Valdivia A, Kong M, Alvarez A, Cardenas A, et al. (2013) Thy-1-interacting molecules and cellular signaling in cis and trans. Int Rev Cell Mol Biol 305: 163-216.

[10] Chen Y, Veracini L, Benistant C, Jacobson K (2009) The transmembrane protein CBP plays a role in transiently anchoring small clusters of Thy-1, a GPI-anchored protein, to the cytoskeleton. J Cell Sci 122: 3966-3972.

[11] Brdicka T, Pavlistova D, Leo A, Bruyns E, Korinek V, et al. (2000) Phosphoprotein associated with glycosphingolipid-enriched microdomains (PAG), a novel ubiquitously expressed transmembrane adaptor protein, binds the protein tyrosine kinase Csk and is involved in regulation of T cell activation. J Exp Med 191: 1591-1604.

[12] Fiore VF, Strane PW, Bryksin AV, White ES, Hagood JS, et al. (2015) Conformational coupling of integrin and Thy-1 regulates Fyn priming and fibroblast mechanotransduction. J Cell Biol 211: 173-190.

[13] Simons K, Toomre D (2000) Lipid rafts and signal transduction. Nat Rev Mol Cell Biol 1: 31-39.

[14] Solheim SA, Torgersen KM, Tasken K, Berge T (2008) Regulation of FynT function by dual domain docking on PAG/CBP. J Biol Chem 283: 2773-2783.

[15] Wong L, Lieser SA, Miyashita O, Miller M, Tasken K, et al. (2005) Coupled motions in the SH2 and kinase domains of Csk control Src phosphorylation. J Mol Biol 351: 131-143.

[16] Lindquist S, Karitkina D, Langnaese K, Posevitz-Fejfar A, Schraven B, et al. (2011) Phosphoprotein Associated with Glycosphingolipid-Enriched Microdomains Differentially Modulates Src Kinase Activity in Brain Maturation. PLoS One 6: e23978.

[17] Brouns MR, Matheson SF, Hu KQ, Delalle I, Caviness VS, et al. (2000) The adhesion signaling molecule p190 RhoGAP is required for morphogenetic processes in neural development. Development 127: 4891-4903.

[18] Brouns MR, Matheson SF, Settleman J (2001) p190 RhoGAP is the principal Src

substrate in brain and regulates axon outgrowth, guidance and fasciculation. Nat Cell Biol 3: 361-367.
[19] Fincham VJ, Chudleigh A, Frame MC (1999) Regulation of p190 Rho-GAP by v-Src is linked to cytoskeletal disruption during transformation. J Cell Sci 112: 947-956.
[20] Arthur WT, Petch LA, Burridge K (2000) Integrin engagement suppresses RhoA activity via a c-Src-dependent mechanism. Curr Biol 10: 719-722.
[21] Jeon CY, Moon MY, Kim JH, Kim HJ, Kim JG, et al. (2012) Control of neurite outgrowth by RhoA inactivation. J Neurochem 120: 684-698.
[22] Jeon C-Y, Kim H-J, Morii H, Mori N, Settleman J, et al. (2010) Neurite outgrowth from PC12 cells by basic fibroblast growth factor (bFGF) is mediated by RhoA inactivation through p190RhoGAP and ARAP3. J Cell Physiol 224: 786-794.
[23] Maciver SK, Hussey PJ (2002) The ADF/cofilin family: actin-remodeling proteins. Genome Biol 3: reviews3007.
[24] Riento K, Ridley AJ (2003) Rocks: multifunctional kinases in cell behaviour. Nat Rev Mol Cell Biol 4: 446-456.
[25] Herrera-Molina R, Frischknecht R, Maldonado H, Seidenbecher CI, Gundelfinger ED, et al. (2012) Astrocytic αvβ3 integrin inhibits neurite outgrowth and promotes retraction of neuronal processes by clustering Thy-1. PLoS One 7: e34295.
[26] Chavis P, Westbrook G (2001) Integrins mediate functional pre- and postsynaptic maturation at a hippocampal synapse. Nature 411: 317-321.
[27] Zhang F, Crise B, Su B, Hou Y, Rose JK, et al. (1991) Lateral diffusion of membrane-spanning and glycosylphosphatidylinositol-linked proteins: toward establishing rules governing the lateral mobility of membrane proteins. J Cell Biol 115: 75-84.
[28] Trimble WS, Grinstein S (2015) Barriers to the free diffusion of proteins and lipids in the plasma membrane. J Cell Biol 208: 259-271.
[29] Castro JB, Gould TJ (2015) Neuro at the Nanoscale: Diffraction-Unlimited Imaging with STED Nanoscopy. J Histochem & Cytochem 63: 897-907.
[30] Tam J, Merino D (2015) Stochastic optical reconstruction microscopy (STORM) in comparison with stimulated emission depletion (STED) and other imaging methods. J Neurochem 135: 643-658.
[31] Narisawa-Saito M, Yamanashi Y, Morioka T, Oite T, Shimizu F (1996) Thy-1 molecule associates with protein tyrosine kinase(s) in rat mesangial cells. Clin Exp Immunol 106: 86-90.
[32] Hueber AO, Bernard AM, Battari CL, Marguet D, Massol P, et al. (1997) Thymocytes in Thy-1-/- mice show augmented TCR signaling and impaired differentiation. Curr Biol 7: 705-708.
[33] Barker TH, Grenett HE, MacEwen MW, Tilden SG, Fuller GM, et al. (2004) Thy-1 regulates fibroblast focal adhesions, cytoskeletal organization and migration through modulation of p190 RhoGAP and Rho GTPase activity. Exp Cell Res 295: 488-496.
[34] Barker TH, Pallero MA, MacEwen MW, Tilden SG, Woods A, et al. (2004) Thrombospondin-1-induced focal adhesion disassembly in fibroblasts requires Thy-1 surface expression, lipid raft integrity, and Src activation. J Biol Chem 279: 23510-23516.
[35] Shan B, Hagood JS, Zhuo Y, Nguyen HT, MacEwen M, et al. (2010) Thy-1 attenuates TNF-α-activated gene expression in mouse embryonic fibroblasts via Src family kinase. PLoS One 5: e11662.
[36] Haskell MD, Nickles AL, Agati JM, Su L, Dukes BD, et al. (2001) Phosphorylation of p190 on Tyr1105 by c-Src is necessary but not sufficient for EGF-induced actin disassembly in C3H10T1/2 fibroblasts. J Cell Sci 114: 1699-1708.
[37] Avalos AM, Arthur WT, Schneider P, Quest AF, Burridge K, et al. (2004) Aggregation of integrins and RhoA activation are required for Thy-1-induced

morphological changes in astrocytes. J Biol Chem 279: 39139-39145.
[38] Burridge K, Wennerberg K (2004) Rho and Rac take center stage. Cell 116: 167-179.
[39] Humphries JD, Byron A, Humphries MJ (2006) Integrin ligands at a glance. J Cell Sci 119: 3901-3903.
[40] Hynes RO (2002) Integrins: bidirectional, allosteric signaling machines. Cell 110: 673-687.
[41] Albelda SM, Buck CA (1990) Integrins and other cell adhesion molecules. The FASEB Journal 4: 2868-2880.
[42] Avalos AM, Valdivia AD, Munoz N, Herrera-Molina R, Tapia JC, et al. (2009) Neuronal Thy-1 induces astrocyte adhesion by engaging syndecan-4 in a cooperative interaction with αvβ3 integrin that activates PKCα and RhoA. J Cell Sci 122: 3462-3471.
[43] Leyton L, Schneider P, Labra CV, Ruegg C, Hetz CA, et al. (2001) Thy-1 binds to integrin β3 on astrocytes and triggers formation of focal contact sites. Curr Biol 11: 1028-1038.
[44] Henriquez M, Herrera-Molina R, Valdivia A, Alvarez A, Kong M, et al. (2011) ATP release due to Thy-1-integrin binding induces P2X7-mediated calcium entry required for focal adhesion formation. J Cell Sci 124: 1581-1588.
[45] Garcia-Parajo MF, Cambi A, Torreno-Pina JA, Thompson N, Jacobson K (2014) Nanoclustering as a dominant feature of plasma membrane organization. J Cell Sci 127: 4995-5005.
[46] Goswami D, Gowrishankar K, Bilgrami S, Ghosh S, Raghupathy R, et al. (2008) Nanoclusters of GPI-anchored proteins are formed by cortical actin-driven activity. Cell 135: 1085-1097.
[47] Stefanova I, Horejsi V, Ansotegui IJ, Knapp W, Stockinger H (1991) GPI-anchored cell-surface molecules complexed to protein tyrosine kinases. Science 254: 1016-1019.
[48] Mahanthappa NK, Patterson PH (1992) Thy-1 multimerization is correlated with neurite outgrowth. Dev Biol 150: 60-71.
[49] Mahanthappa NK, Patterson PH (1992) Thy-1 involvement in neurite outgrowth: perturbation by antibodies, phospholipase C, and mutation. Dev Biol 150: 47-59.
[50] Perkins SJ, Williams AF, Rademacher TW, Dwek RA (1988) The Thy-1 glycoprotein: a three-dimensional model. Trends Biochem Sci 13: 302-303.
[51] Hermosilla T, Muñoz D, Herrera-Molina R, Valdivia A, Muñoz N, et al. (2008) Direct Thy-1/αvβ3 integrin interaction mediates neuron to astrocyte communication. Biochim Biophys Acta (BBA) 1783: 1111-1120.
[52] Choi J, Leyton L, Nham SU (2005) Characterization of αX I-domain binding to Thy-1. Biochem Biophys Res Commun 331: 557-561.
[53] Fiore VF, Ju L, Chen Y, Zhu C, Barker TH (2014) Dynamic catch of a Thy-1-α5β1+syndecan-4 trimolecular complex. Nat Commun 5: 4886.
[54] Saalbach A, Wetzel A, Haustein UF, Sticherling M, Simon JC, et al. (2005) Interaction of human Thy-1 (CD 90) with the integrin αvβ3 (CD51/CD61): an important mechanism mediating melanoma cell adhesion to activated endothelium. Oncogene 24: 4710-4720.
[55] Zhou Y, Hagood JS, Lu B, Merryman WD, Murphy-Ullrich JE (2010) Thy-1-Integrin αvβ5 Interactions Inhibit Lung Fibroblast Contraction-induced Latent Transforming Growth Factor-β1 Activation and Myofibroblast Differentiation. J Biol Chem 285: 22382-22393.
[56] Jiang LQ, Feng X, Zhou W, Knyazev PG, Ullrich A, et al. (2006) Csk-binding protein (CBP) negatively regulates epidermal growth factor-induced cell transformation by controlling Src activation. Oncogene 25: 5495-5506.

[57] Saka SK, Honigmann A, Eggeling C, Hell SW, Lang T, et al. (2014) Multi-protein assemblies underlie the mesoscale organization of the plasma membrane. Nat Commun 5: 4509.
[58] Kanou T, Oneyama C, Kawahara K, Okimura A, Ohta M, et al. (2011) The transmembrane adaptor CBP/PAG1 controls the malignant potential of human non-small cell lung cancers that have c-src upregulation. Mol Cancer Res 9: 103-114.
[59] Hrdinka M, Horejsi V (2014) PAG--a multipurpose transmembrane adaptor protein. Oncogene 33: 4881-4892.
[60] Brdičková N, Brdička T, Anděra L, Špička J, Angelisová P, et al. (2001) Interaction between two adapter proteins, PAG and EBP50: a possible link between membrane rafts and actin cytoskeleton. FEBS Lett 507: 133-136.
[61] Itoh K, Sakakibara M, Yamasaki S, Takeuchi A, Arase H, et al. (2002) Cutting Edge: Negative Regulation of Immune Synapse Formation by Anchoring Lipid Raft to Cytoskeleton Through CBP-EBP50-ERM Assembly. J Immunol 168: 541-544.
[62] Fujita Y, Yamashita T (2014) Axon growth inhibition by RhoA/ROCK in the central nervous system. Front Neurosci 8: 338.
[63] Sebök Á, Nusser N, Debreceni B, Guo Z, Santos MF, et al. (1999) Different Roles for RhoA During Neurite Initiation, Elongation, and Regeneration in PC12 Cells. J Neurochem 73: 949-960.
[64] Herrera-Molina R, Sarto-Jackson I, Montenegro-Venegas C, Heine M, Smalla KH, et al. (2014) Structure of Excitatory Synapses and GABAA Receptor Localization at Inhibitory Synapses Are Regulated by Neuroplastin-65. J Biol Chem 289: 8973-8988.
[65] Biermann B, Sokoll S, Klueva J, Missler M, Wiegert JS, et al. (2014) Imaging of molecular surface dynamics in brain slices using single-particle tracking. Nat Commun 5.

SUPPLEMENTARY MATERIAL

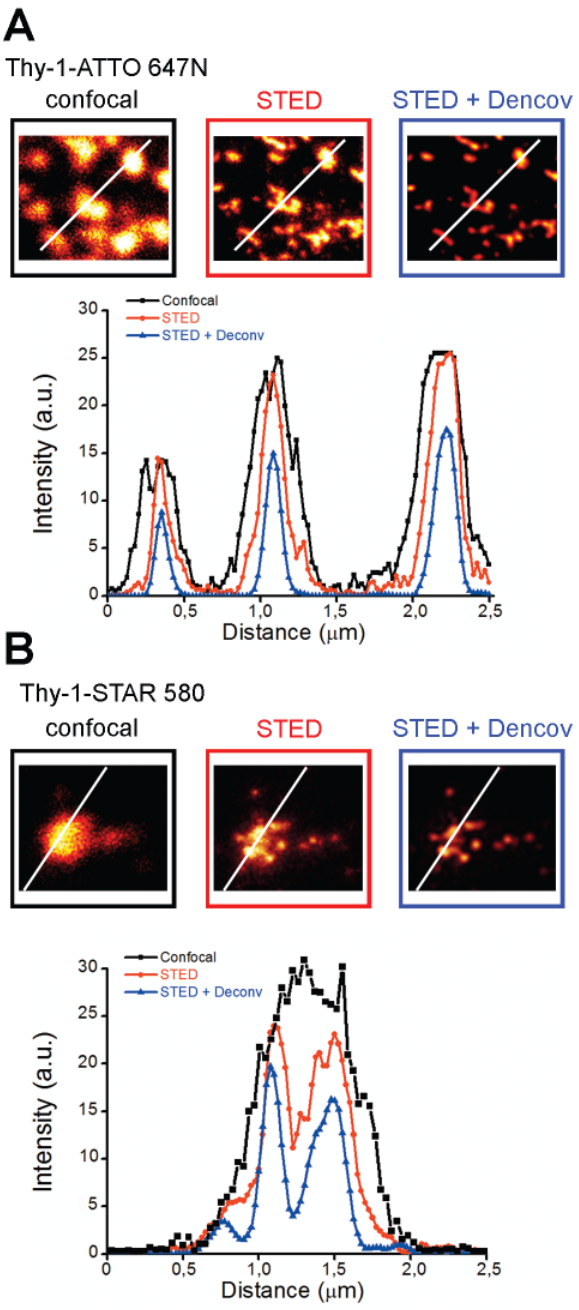

Supplementary Figure S1: Super-resolution visualization of Thy-1 nanoclusters by STED microscopy and image deconvolution.

(A and B) Cultured cortical neurons were stained with an anti-Thy-1 antibody (see Methods). Either ATTO 647N- (A) or STAR 580-conjugated (B) secondary antibodies were employed to indirectly detect Thy-1. Thy-1 nanoclusters were visualized in confocal (black line) or STED mode (red line). STED images were deconvolved using STED tools in Huygens software (STED + Deconv; blue line). White lines (2.5 μm long) in images represent the line scans where the fluorescence intensity profile was quantified using ImageJ software (line scans starting left of images). For each scan, plots of fluorescence intensity versus distance were generated.

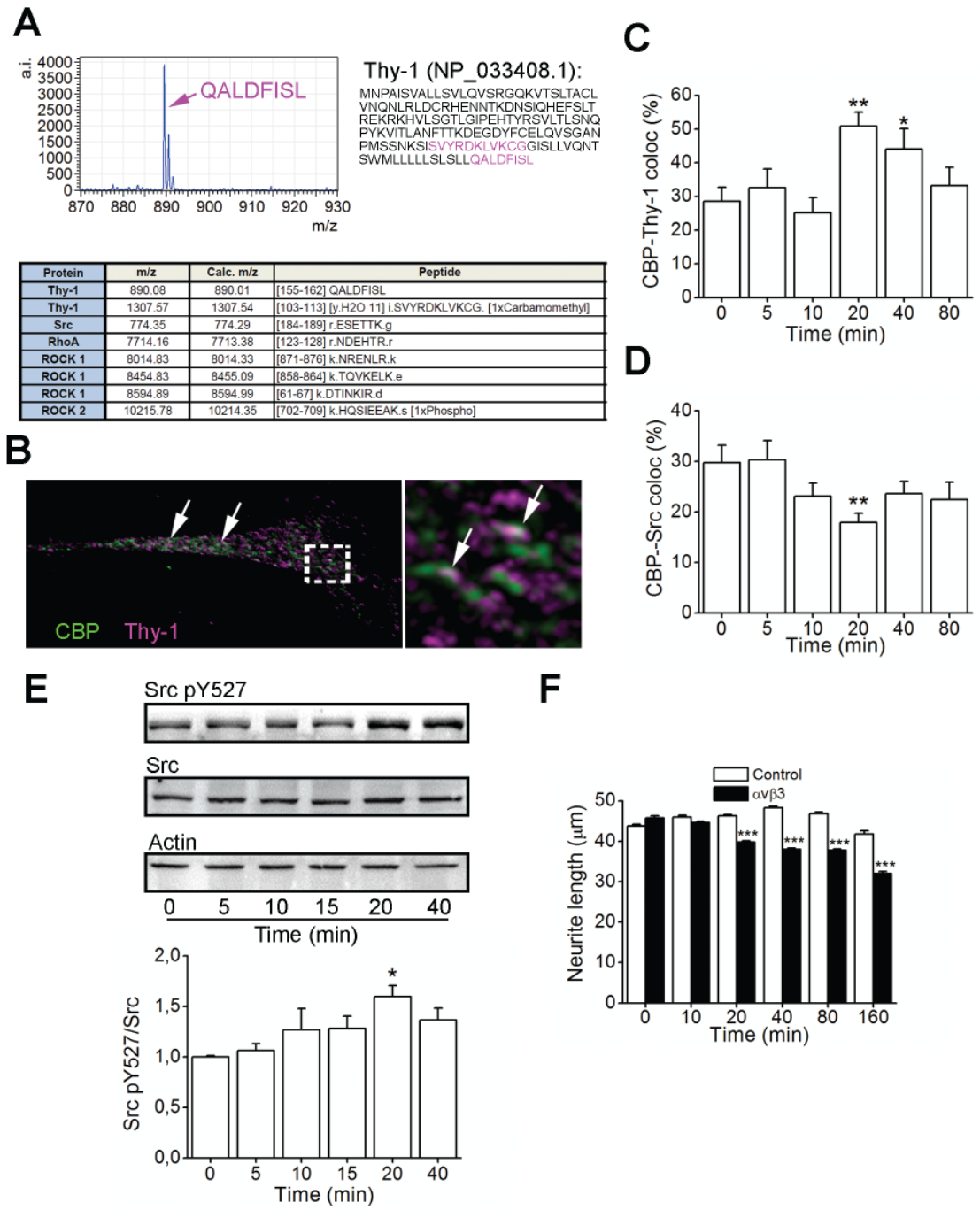

Supplementary Figure S2: αvβ3 integrin triggers neurite retraction and Src inactivation in CAD cells.

(A) Maldi-TOF analysis of Thy-1-containing immunoprecipitates. Thy-1 peptides were detected (peak on the mass spectra) and confirmed by comparison with the Thy-1 sequence (highlighted in magenta; NP_033408.1). In the table, identification parameters of Thy-1 and other detected peptides are provided. **(B)** Deconvolved confocal image of Thy-1 (magenta) and CBP (green) in neurites of differentiated CAD cells. Scale bar = 5 µm. Right image is a digital zoom of the dashed-line area. White arrows indicate co-localized clusters. **(C and D)** Percentage of co-localization of CBP with Thy-1 (C) or Src (D) calculated from images obtained as in B of CAD cells stimulated with αvβ3 integrin. Ten pictures were measured per condition, per experiment. *p<0.05, **p<0.01 versus control. **(E)** Cell lysates of differentiated

CAD cells, which were stimulated with αvβ3 integrin for different time periods, were immunoblotted for Src pY527, Src, and actin. The graph shows the ratio of Src pY527/Src normalized to actin and expressed as fold change relative to untreated control. Data are presented as mean ± SEM from five independent experiments. *p < 0.05 versus time 0. **(F)** Quantification of neurite lengths of differentiated CAD cells under control and αvβ3 integrin-stimulated conditions for different time periods. Values are presented as mean ± SEM of three independent experiments. The neurites of 100 cells were measured per condition, per experiment. ***p < 0.001 versus control at the same time point.

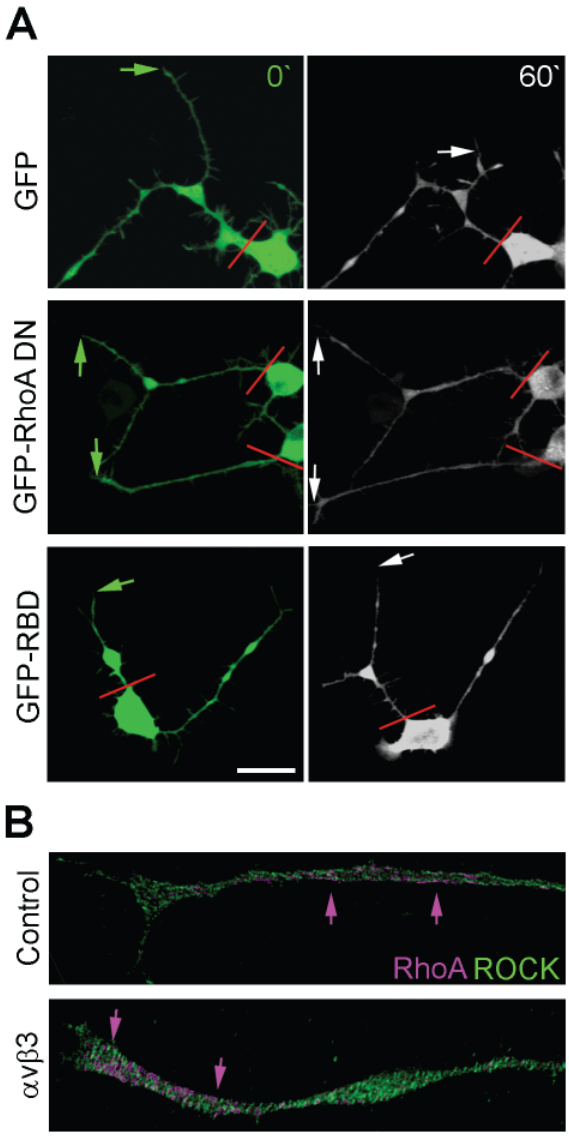

Supplementary Figure S3: RhoA mediates αvβ3 integrin-induced neurite retraction and relocalizes upon integrin stimulation.

(A) Differentiated CAD cells were transfected with GFP, GFP dominant-negative RhoA (GFP-RhoA DN), or GFP-RBD, and then stimulated with αvβ3 integrin. Images obtained by time-lapse video microscopy at time 0 (green) and 60 min (white) are shown. Red lines indicate the beginning of a neurite from the cell soma, and the arrows indicate the neurite tip at time 0 (green) and 60 min (white). Scale bar = 20 μm. **(B)** Deconvolved confocal images of ROCK (green) and RhoA (magenta) for neurites of differentiated CAD cells under control conditions (Control) or after stimulation with αvβ3 integrin (αvβ3) for 20 min. Magenta arrows indicate RhoA localization.

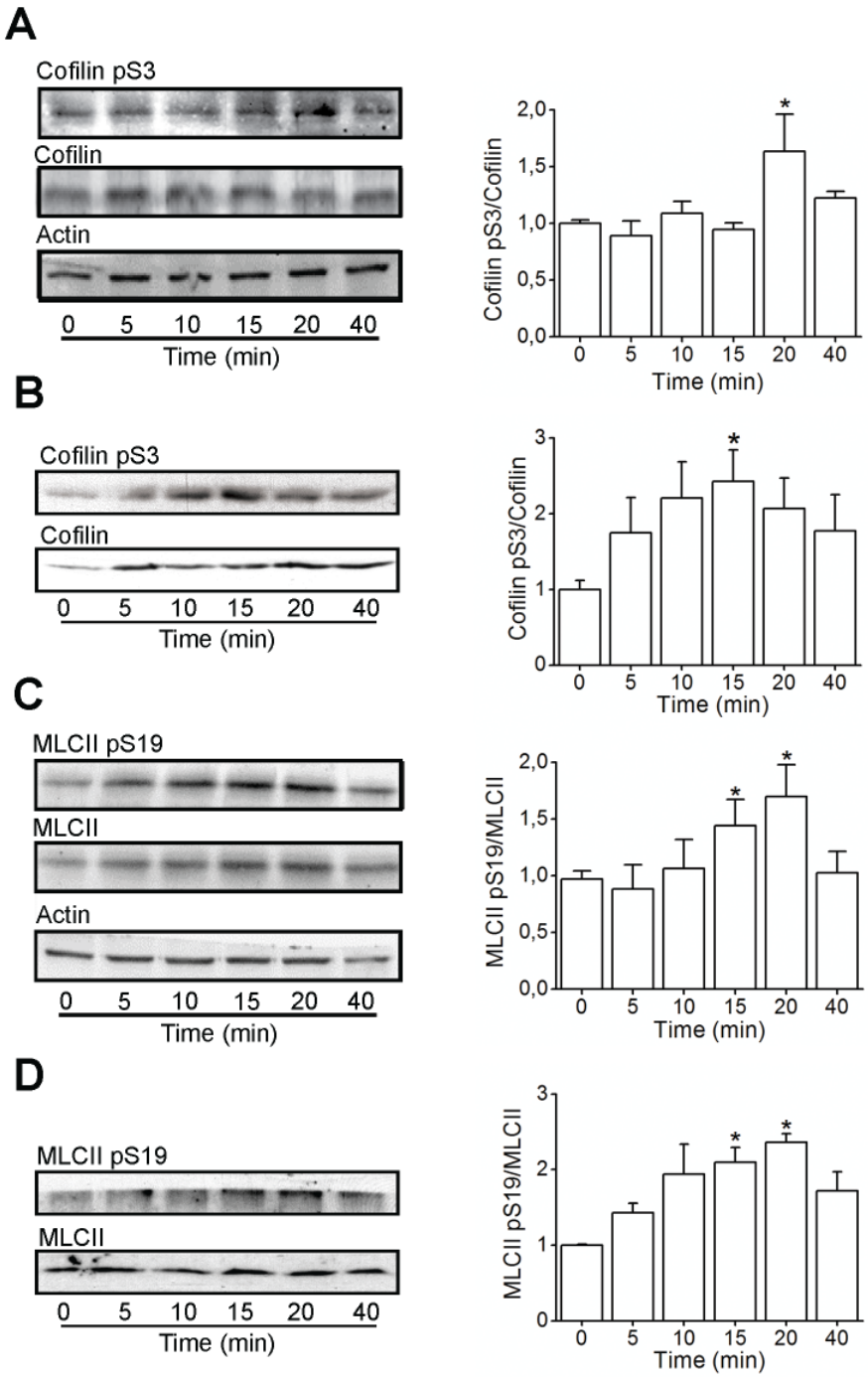

Supplementary Figure S4: αvβ3 integrin increases cofilin and MLCII phosphorylation in CAD cells and cortical neurons.

(A–D) Cell lysates from αvβ3 integrin-stimulated CAD cells (A and C) and cortical neurons (B and D) were immunoblotted for phosphoserine 3 (pS3) and total cofilin (A and B) or phosphoserine 19 (pS19) and total MLCII (C and D). Actin is shown as a control for protein loading (A and C). Values in the graphs are the phosphorylated/total protein ratios expressed as fold change relative to values at time point 0. Data are the mean ± SEM from three independent experiments. *$p < 0.05$ versus time.